NASA TECHNICAL NOTE

NASA TN D-2424

BREAKUP OF A LIQUID JET
IN A TRANSVERSE FLOW OF GAS

by Bruce J. Clark

Lewis Research Center

Cleveland, Ohio

BREAKUP OF A LIQUID JET IN A TRANSVERSE FLOW OF GAS

By Bruce J. Clark

Lewis Research Center
Cleveland, Ohio

NATIONAL AERONAUTICS AND SPACE ADMINISTRATION

BREAKUP OF A LIQUID JET IN A TRANSVERSE FLOW OF GAS

by Bruce J. Clark

Lewis Research Center

SUMMARY

The breakup of a water jet exposed to a flow of nitrogen at right angles to it has been demonstrated by photographs and by measurement of its electrical resistance. The photographs show that the jet spreads progressively transverse to the flow of gas and that drops and ligaments tear off along the edges of the thinned out jet. The electrical resistance of the jet increases as this breakup progresses and is a measure of the cross-sectional area of the portion of the jet remaining intact. As measured by the electrical resistance, the degree of liquid breakup is correlated graphically with the parameters influencing the breakup. By differentiating the expression for the resistance with respect to jet length, the following expression is obtained for relative cross-sectional area remaining at any point in the jet:

$$\frac{A}{A_O} = [0.00392(7.68\epsilon - 1)(\epsilon - 1)^{2.34} + 1]^{-1}$$

where $\epsilon = \dfrac{\rho_g}{\rho_l}\left(\dfrac{VL}{v_l D_O}\right)^2 = \dfrac{\rho_g}{\rho_l}\left(\dfrac{Vt}{D_O}\right)^2$, ρ_g is gas density, ρ_l is liquid density,

$V = \sqrt{U^2 + v_l^2}$ is relative velocity between gas and liquid, v_l is liquid velocity, D_O is liquid jet diameter, L is distance over which liquid is acted upon by gas, and t is time during which liquid is acted upon by gas.

The photographs of the spreading liquid and the form of the correlating parameter ϵ for degree of breakup support the view that, because of the gas flow, an external pressure distribution exists around the jet that is similar to that around a solid cylinder. The liquid responds inertially to this accelerating force, with surface tension and viscosity effects being negligible at reasonably high Weber and Reynolds numbers. The turbulence-produced roughness of the jet is adequate to make the jet see a total gas velocity equal to the vector sum of gas and liquid velocities, so that distortion rate is proportional to $U^2 + v_l^2$ and not U^2 alone.

Application of these results to other jet and drop breakup data, although obtained under widely varying conditions, results in an approximate correlation of those results.

INTRODUCTION

Recently, considerable attention has been given to the physical process of injection and its role in the control of the rate and/or completeness of combustion (refs. 1 to 5). Most of the interest has been concentrated on the drop sizes produced by different types of injectors under various environmental conditions. Some work has been performed to determine how the atomization process that produces the drops can be modified or completely changed in character by environmental changes (ref. 6). Comparatively little has been reported on the rate of the breakup process itself and how this rate is influenced by such variables as densities, velocities, and injector and combustor geometry.

Jet-penetration studies have been made for many years with the objective of predicting maximum travel of a fire-hose spray and minimum length of free jet necessary to avoid electrical shock hazard (refs. 7 to 10). Similar studies have been made with agricultural sprays and oil burner sprays (refs. 11 and 12). Considerable work has been done on the length and the rate of penetration of the spray from a diesel injector into the combustion chamber (refs. 11 to 14). In those studies, the surrounding gas was stagnant except for the flow induced by the liquid jet.

Mass distribution and drop size measurements have been made for the breakup of fuel jets in a crosscurrent flow of gas (ref. 15). Earlier investigators (ref. 16) showed pictures of breakup at low velocities in crosscurrent flow. Others (refs. 17 to 36) have studied the behavior of drops and sprays in the gas flow in a shock tube or blast gun or in different types of tunnels.

In steady-state combustion, the rate of liquid breakup, as well as the vaporization rate, is important in predicting the total time or length required for complete combustion. In oscillatory combustion, a possible mechanism for amplifying the instability is the increase in energy release rate caused by more rapid atomization immediately behind the pressure wave. The prediction of local heat release and heat-transfer rates also requires a knowledge of the liquid breakup rate.

In this study the particular case of a cylindrical liquid jet formed by a simple orifice and atomized by a transverse flow of gas is investigated experimentally by measuring its electrical resistance. The significant parameters varied are gas density, gas velocity, liquid velocity, orifice diameter, and distance along the jet over which the gas flow impinges on the liquid. Results are correlated in terms of a parameter derived from a suggested mechanism by which breakup occurs. Atomization or breakup rate for any point in the jet can be calculated from the experimental data.

SYMBOLS

A cross-sectional area of liquid jet

A_0 original cross-sectional area of liquid jet

a	nonaxial acceleration of liquid in jet
D_{max}	maximum observed droplet diameter
D_O	liquid jet diameter
D_{30}	volume-median droplet diameter
d_a	effective action distance indicated by velocity profile
g	acceleration due to gravity
L	distance from injector exit over which liquid is acted upon by gas
L_O	length of liquid injector hole
N	correction factor for nonuniform gas velocity and for length-averaging of ϵ
P_g	pressure in gas phase, lb/sq in. gage
p	pressure in liquid phase
p_σ	local contribution of surface tension to liquid-phase pressure
R	electrical resistance of given length of liquid jet
Re	Reynolds number, $(D_O U \rho_g)/\mu_g$
R_O	calculated resistance of given length of undistorted liquid jet
r_1, r_2	principal radii of curvature of surface
s	distance in unspecified direction
t	time liquid has been exposed to gas flow
U	gas velocity
V	relative velocity of gas with respect to the liquid, $\sqrt{U^2 + v_l^2}$
v_l	axial velocity of liquid jet
W	total width of liquid jet after spreading
We	Weber number, $(\rho_g U^2 D_O)/\sigma$
w	nonaxial velocity in liquid phase
x	distance in direction of liquid injection

y distance in direction of gas flow

δ maximum displacement of liquid in its distorted cross section

ϵ relative distortion of liquid jet cross section,

$$\delta/D_o = \frac{\rho_g}{\rho_l}\left(\frac{VL}{v_l D_o}\right)^2 = \frac{\rho_g}{\rho_l}\left(\frac{Vt}{D_o}\right)^2$$

ϵ_{av} length average of ϵ, $N\dfrac{\rho_g}{\rho_l}\left(\dfrac{V_{max}L}{v_l D_o}\right)^2$

λ_L $\dfrac{\rho_g}{\rho_l}\left(\dfrac{V}{v_l D_o}\right)^2 = \dfrac{\epsilon}{L^2}$

λ_t $\dfrac{\rho_g}{\rho_l}\left(\dfrac{V}{D_o}\right)^2 = \dfrac{\epsilon}{t^2}$

μ absolute viscosity

ξ nondimensional distance along liquid jet, x/L

ρ density

ρ_E electrical resistivity

σ surface tension

Subscripts:

b   at complete breakup

g   in gas phase

i   at initiation of breakup

l in liquid phase

max   maximum

EQUIPMENT AND PROCEDURE

The general arrangement of the test apparatus is shown in figure 1. A 5-inch pipe tee is fitted with windows on each end and a drain valve at the bottom. Nitrogen gas and water are introduced near the top. Details of the impingement zone are shown in figure 2. The longitudinal baffle reduces the

amount of vortexing induced by the high velocity gas.

Two different gas injectors were used to provide variations in the action distance over which the gas flow reacts with the stream of water (fig. 3). By rotating these injectors 90° (designated I' and II'), four different action distances could be used. The gas velocity profiles of these injectors were measured by a total head probe and are shown in figure 4. The total head probe was simply a vertical tube, 1/8 inch in diameter and closed at the bottom end. Total head was sensed through a 0.04-inch hole drilled through the side, 1/2 inch from the end. An effective action distance d_a for each injector was taken from the width of the velocity profile at 70 percent of maximum velocity; this effective action distance was used only for approximate comparisons between gas injectors. The velocity of the injected gas was controlled by critical flow nozzles as shown in figure 1. Flow nozzle sizes and approximate values of resultant velocities in the gas injectors are listed in the following table:

Diameter of flow nozzle, in.	Gas velocity, U, ft/sec	
	Gas injector	
	I and I'	II and II'
0.440	548	310
.390	430	245
.360	365	208
.312	273	155
.281	220	125
.249	173	98
.204	115	65
.1695	78	---
.1405	52	---

Gas pressure was controlled by a regulator and measured by a strain gage, and gas temperature was measured by a bare-wire thermocouple.

The water injectors (fig. 3(b)) were made of 0.065-, 0.089-, and 0.120-inch inside-diameter tubing, with length to diameter ratios of 19, 14, and 10.4, respectively. All had sharp-edged approach sections. An additional water injector was made of 0.089-inch inside-diameter tubing with a length to diameter ratio of 100. Data from this injector are shown in the photographs but not in the correlated data.

Water flow was controlled by pressurizing a tank and measured by a turbine-type flowmeter. Water pressure and temperature were taken by strain gage and thermocouple.

A movable electrical probe screen (refs. 7, 37, and 38) at either 300 or 67.5 volts d-c potential was used to measure the electrical conduction of the

5

water stream from water injector to screen (fig. 2). The electrical circuit for these measurements is shown in figure 5. The conductivity of tap water was such that the jet resistance was of the order of 1 megohm. For each particular jet diameter and length, measured values of the undistorted jet resistance with no gas velocity were averaged for the values of R_O used in correlating the data. Because of cavitation and turbulence effects on the jet cross section, these measured resistances with no gas velocity averaged 30 percent above those calculated for a smooth cylinder using the measured conductivity of the water. Tests were made in a conductivity tube (fig. 5) at various current densities and liquid velocities to ensure that there were no polarization or velocity effects on the ionic conductivity of the water.

Resistance readings and photographs were taken during relatively short periods of water flow, while the gas flow was steady. This procedure was necessary to avoid serious electrical short circuiting from the probe screen to the walls.

For different gas injectors, the screen position was changed to coincide with the point where the gas velocity had dropped off to 70 percent of the maximum.

Photographs of breakup at various conditions were taken with a 4 by 5 camera with Polaroid back, using 3000 speed film. Pictures were taken with a 20-inch f/5.6 lens and with a $12\frac{1}{2}$-inch f/6.3 lens. A diffuse screen was used for backlighting, illuminated by a 1/2-microsecond 7-joule air spark. Depth of field was necessarily small to keep the droplets on the chamber windows completely out of focus. The mirror arrangement shown in figure 1 was used to obtain the two perpendicular views of the breakup simultaneously.

MODEL OF BREAKUP PROCESS

The model proposed in this report for the controlling mechanism of breakup of a liquid jet in a crosscurrent flow of gas can be deduced from a consideration of the internal and external forces acting on the liquid. Contributing to the breakup process are the normal and tangential components of the dynamic pressure of the flowing gas on the liquid surface. These tend to bend the liquid stream in the direction of the gas flow, to distort the cross-sectional shape of the liquid, and to tear liquid off from the surface at particular regions along the stream periphery. The surface tension of the liquid tends initially to restore the liquid to its original cross-sectional shape; however, in the later stages of breakup, it actually assists in the process of disintegration. Considerable turbulence is generated in the liquid in the entry region of the injector, and this contributes to the surface roughness of the liquid as it emerges from the tube or orifice. The viscosity of the liquid resists all relative motion within the liquid, and hence retards the effects of the external, surface, and turbulent forces.

To evaluate the external forces on the liquid, it is assumed that the boundary layer and wake formed in the gas phase are similar to those formed

under steady-state conditions about a solid cylinder of similar size. References 39 to 42 present measured data for the pressure distribution around comparatively large circular cylinders (fig. 6). Both the normal and the tangential stress components are given as fractions of the dynamic pressure of the gas $\rho_g U^2$. The maximum tangential stress occurs at about the place on the circumference that separation occurs; however, this tangential stress is two or three orders of magnitude less than the normal pressure exerted on the cylinder. Hence, the normal component will be primarily responsible for distorting a liquid cylinder, while the tangential component will probably be adequate to shred off some liquid at the point where the boundary layer separates. Figure 6 presents the normal pressure data of reference 39 obtained for a 3-inch cylinder in a wind tunnel at a Reynolds number in the range of this study. Shown also is the normal pressure distribution around a 1/8-inch cylinder measured in the present study by rotating the total head probe. In spite of differences in the gas stream and cylinder size, the measured distributions are quite similar. The maximum difference in pressure is between the stagnation point and the points of separation on each side and is about twice the dynamic pressure.

The actual liquid jet is not a smooth cylinder except at very low flows, but presents a rough surface to the gas flow (refs. 37 and 43). At the stagnation point on each rough protuberance, the dynamic pressure would be $\rho_g(U^2 + v_l^2)$, from the vector sum of the gas and liquid velocities, rather than $\rho_g U^2$.

In addition to these effects, gas-phase turbulence and irregular vortex shedding in the wake of the liquid cylinder will produce waviness in the jet.

Surface tension of the liquid tries to maintain a circular cross section of the jet. The pressure generated by the surface tension is

$$p_\sigma = \sigma\left(\frac{1}{r_1} + \frac{1}{r_2}\right)$$

where σ is the surface tension and r_1 and r_2 are the principal radii of curvature of the surface. The surface-tension pressure within a smooth liquid jet is then $2\sigma/D_o$. The pressure will be locally higher at a small protuberance; thus, the protuberance tends to smooth out. If the protuberance grows to a ligament with its length greater than its diameter, surface tension produces a higher pressure in the "neck" so that the ligament is pinched off. For the pressure generated by surface tension to be the magnitude of the dynamic pressure, the radius of curvature would have to be about one one-thousandth of the liquid jet radius. The Weber number $We = (\rho_g U^2 D_o)/\sigma$ expresses the ratio of dynamic forces to surface-tension forces. For a cylinder these forces are equal at a Weber number of 4. High Weber numbers indicate that surface-tension forces are negligible compared to external dynamic forces. In this study the Weber numbers are relatively high, and surface-tension forces are neglected.

If relative gas velocity V, gas density ρ_g, liquid density ρ_l, liquid jet diameter D_O, and action time t are assumed to be the important variables affecting the breakup of a liquid jet, a dimensionless number $(\rho_g/\rho_l)(Vt/D_O)^2$ can be formed, which expresses the ratio of the external dynamic forces to the inertial resistance of the liquid for a given deformation rate.

This same dimensionless number can be derived by integration of the momentum equation for the liquid phase, assuming that the pressure gradient can be taken constant with time:

$$\bar{a} = \frac{d\bar{w}}{dt} = \frac{1}{\rho_l} \nabla p - \frac{\mu_l}{\rho_l} \nabla^2 \bar{w} + \bar{g} \tag{1}$$

Let

$$|\nabla p| \approx \frac{\Delta p}{\Delta s} \approx \frac{2\left(\frac{1}{2}\rho_g V^2\right)}{\frac{1}{2}D_O} = 2\frac{\rho_g V^2}{D_O} \tag{2}$$

where $2\left(\frac{1}{2}\rho_g V^2\right)$ represents the pressure difference Δp between stagnation and and separation points. The distance Δs between these points is initially $\frac{1}{2}D_O$, increases during the first stage of deformation to around $\frac{3}{2}D_O$, and then decreases to zero as breakup approaches completion. Thus, $\frac{1}{2}D_O$ is taken as an approximate average value of Δs.

By order-of-magnitude analysis of the momentum equation, it can be shown that the viscous term is about four orders of magnitude less than the pressure term for conditions typical of these experiments, and the gravitational term is even smaller. Hence, gravitational and viscous effects are neglected. Then the acceleration of the liquid in a direction transverse to the gas flow can be approximated by

$$a = 2\frac{\rho_g}{\rho_l}\frac{V^2}{D_O} \tag{3}$$

By integration,

$$w = 2\frac{\rho_g}{\rho_l}\frac{V^2}{D_O}t \tag{4}$$

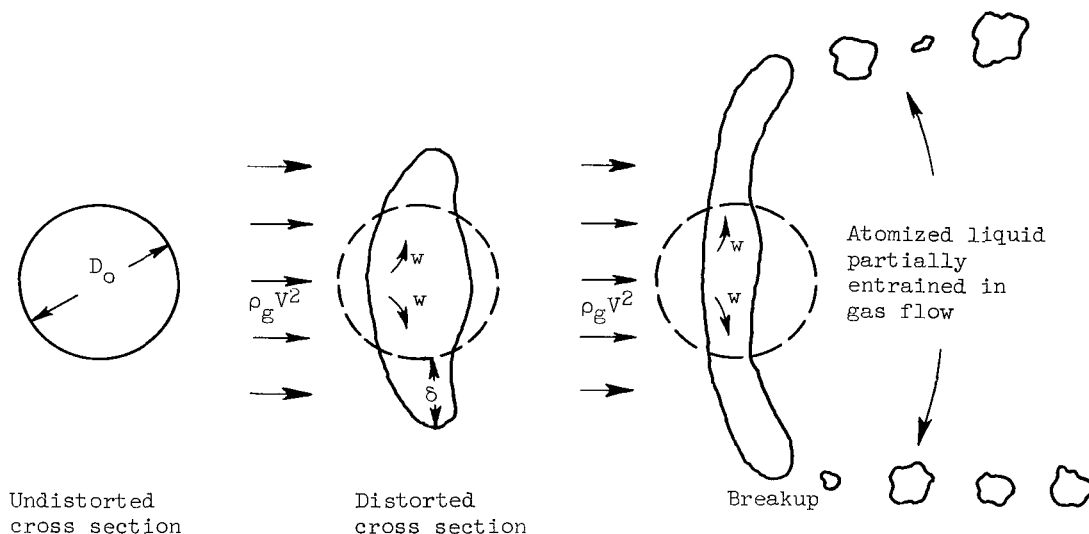$$\delta = \frac{\rho_g}{\rho_l}\frac{V^2}{D_O}t^2 \tag{5}$$

Let

$$\epsilon = \frac{\delta}{D_O} = \frac{\rho_g}{\rho_l}\left(\frac{Vt}{D_O}\right)^2 \tag{6}$$

8

The parameter ϵ is then the relative distortion of the liquid cross section, and the transverse spreading of the jet is then

$$W = D_O + 2\delta = D_O(1 + 2\epsilon) \tag{7}$$

Numerical integration for the above equations with Δs dependent on the degree of distortion indicates that the correction to W would be less than 30 percent.

The following sketch illustrates the proposed model for this primary mechanism of breakup of a liquid jet in a cross flow of gas:

D_O $\rho_g V^2$ w δ $\rho_g V^2$ w Atomized liquid partially entrained in gas flow

Undistorted cross section   Distorted cross section   Breakup

The external pressure distribution creates a pressure gradient within the liquid, resulting in flattening of the liquid jet transverse to the flow of gas. At the edges of this flattened sheet drops and ligaments are torn off by the combined action of the tangential stress and surface tension. The rate of breakup is assumed to be controlled by the distortion rate of the liquid cross section. High viscosity will retard the distortion, but the controlling step should remain the same. This model would not apply for the cases where surface forces are comparable to dynamic forces, resulting in low Weber numbers.

EXPERIMENTAL RESULTS

Evidence of the degree of liquid breakup is presented in photographs and in terms of electrical resistance. Photographs showing the independent effects of the various factors affecting breakup are presented in figures 7 to 11. For comparison, the electrical resistance of the water jet is given, where R_O is the average measured resistance of the undistorted jet with no gas velocity. It is evident that degree of breakup and resistance both increase directly with gas velocity U (fig. 9), density (or pressure P_g) (fig. 8), and effective

action distance d_a (fig. 11). Breakup and resistance vary inversely with liquid velocity v_l (fig. 7) and jet diameter D_o (fig. 10). At low degrees of breakup the effect on electrical resistance is masked by variations in initial roughness of the jet, which also causes an increase in the total resistance (see fig. 10).

The mechanism of breakup becomes clearer from photographs taken along the axis of gas flow (fig. 12). Spreading of the liquid jet transverse to the flow of gas increases with gas density and decreases with jet velocity. At the left in each photograph at the same scale is the liquid spreading pattern calculated from the distortion rate predicted by the model (eq. (7)). These are seen to correspond fairly well in magnitude and trend with the photographs. Other photographs taken at very low liquid velocities and gas densities show spreading of the jet and a distinct thinning of the jet in the other cross-sectional dimension.

The assumptions in the model regarding the type of distortion undergone by the liquid during the breakup process are thus borne out by photographic evidence. Stripping off of liquid at the edges of the jet, as assumed in the model, is shown in the pictures. Also, the electrical resistance is shown to correspond closely with the observed degree of breakup.

To check the relative effects of gas density, gas velocity, and liquid jet diameter experimentally, preliminary data were taken with only gas injector II, and adjusting the liquid velocity to give a fixed value of $R/R_o = 3$ (fig. 13). In this case the electrical probe was 0.66 and 0.46 inch from the end of the liquid injector rather than the usual 0.80 inch. Thus, these resistance data cannot be compared directly with those in the photographs or with those presented subsequently.

The following interrelations of several of the experimental factors are shown clearly in the results:

(1) The action time is a function of the dynamic pressure $\rho_g V^2$ exerted by the gas stream.

(2) The vector sum $\sqrt{U^2 + v_l^2}$ of gas and liquid velocities rather than solely the gas velocity is effective in breaking up the jet. This is in agreement with the suggestion in the model presented that a rough-surfaced jet would sense a stagnation pressure dependent on the vector sum of liquid and gas velocities. The ratio of gas to liquid velocities ranges from 0.662 to 5.07. Considerably more spread in the data occurred correlating with $\rho_g U^2$ instead of $\rho_g(U^2 + v_l^2)$.

(3) The rate of breakup is inversely proportional to the diameter squared. This is in contrast to the attempts of other investigators to predict the rate of breakup in terms of Weber number, implying that the larger liquid jet breaks up more easily. This follows from their assumption that the primary resistance to the distorting forces is the surface tension. The cor-

relation of the rate of breakup with $\dfrac{\rho_g}{\rho_l} \dfrac{U^2 + v_l^2}{D_o^2}$, rather than with Weber number

in figure 13 indicates that inertia rather than surface-tension forces controls the rate of breakup; this conclusion is also supported by the photographs in figure 10.

(4) The combined parameter $\dfrac{\rho_g}{\rho_l} \dfrac{U^2 + v_l^2}{D_o^2} t^2$ is constant for the given

degree of breakup $R/R_o = 3$ and the given effective action distance $d_a \approx 0.56$ inch. This invites comparison with the relative distortion

$$\frac{\delta}{D_o} = \epsilon = \frac{\rho_g}{\rho_l} \frac{U^2 + v_l^2}{D_o^2} t^2$$

calculated in terms of the model (eq. (6)).

Similar correlations of action time with $\dfrac{\rho_g}{\rho_l} \dfrac{U^2 + v_l^2}{D_o^2}$ can be made at dif-

ferent degrees of breakup and action distances. The degree of breakup as measured by electrical resistance can then be correlated with the parameter.

$$\epsilon = \frac{\rho_g}{\rho_l} \frac{U^2 + v_l^2}{D_o^2} t^2 = \frac{\rho_g}{\rho_l} \frac{U^2 + v_l^2}{v_l^2} \frac{L^2}{D_o^2} = \frac{\rho_g}{\rho_l} \left(\frac{VL}{v_l D_o}\right)^2$$

In figure 14, this correlation is shown for each of the gas injectors individually. These individual plots are combined in figure 15. In these experiments the gas velocity U did not maintain a constant value over the action distance L, as was shown in figure 4. Therefore, a doubly integrated average of the gas velocity with distance must be used in calculating ϵ (see appendix). The resistance ratio R/R_o will depend on the degree of breakup all along the length of liquid jet, so that a length average ϵ_{av} of the corrected parameter ϵ must be used. The correction factor to ϵ resulting from correcting for the nonuniform gas velocity and averaging the distortion ϵ over the jet length is N.

Data for the 0.065-inch water injector and for gas injector II' show the most scatter. The 0.065-inch water jet also appears to be a little more stable than predicted. The overall spread in the data, as shown in figure 15, is ±25 percent in the low breakup region (excluding ϵ_{av} below 1.0) and ±10 percent in the high breakup region.

An approximate average curve is drawn for all the data; the equation of

this average is

$$R/R_O = 0.00392(3\epsilon_{av} - 1)^{3.34} + 1, \qquad \text{for} \quad \epsilon_{av} \geq 1/3 \qquad (8)$$

During the experiments as ϵ_{av} was decreased by increasing v_l, it was observed that R/R_O approached a constant value of 1 at an ϵ_{av} value of 0.3 to 0.5. The form and constants of equation (8) are chosen to include this characteristic behavior.

The following ranges of individual parameters are included in the data of figures 14 and 15:

Gas velocity, U, ft/sec . . . . 65 to 430
Gas pressure, P_g, lb/sq in. gage . . . . 20 to 250
Liquid velocity, v_l, ft/sec . . . . 15 to 155
Liquid jet diameter, D_O, in. 0.065, 0.089, 0.120
Effective action distance, d_a, in. 0.35, 0.56, 0.70

Weber number, $\dfrac{\rho_g U^2 D_O}{\sigma}$ . . . . 31 to 11,000

Since the minimum Weber number was 31, all of the data were taken under conditions well above the threshold of breakup controlled by surface forces.

Neither liquid jet breakup nor the electrical resistance of the jet are time-steady quantities. Oscilloscope traces of the resistance (fig. 16) show the same kind of high-frequency fluctuations that the photographs of figures 7 to 12 show. Although the resistance varies over at least a 3 to 1 range in these fluctuations, the average appears reasonably close to the average read from the meter. Occasionally the jet breaks completely giving an infinite resistance. At lower jet velocities the complete breaking appears more frequently, although the average resistance remains the same.

Several factors may contribute to the spread in correlated data shown in figure 15. At steady conditions of velocity and pressure repeated measurements in average R/R_O showed a variation of ±10 percent. No modifications were made to the measured R/R_O because of the waving and bending of the liquid jet, although these do increase the electrical path length. Since particular values of $(V/v_l)^2$ were achieved at different liquid velocities, different levels of liquid turbulence are present in one region of the data. With $U = 0$, considerable variation in R_O occurred with changes in v_l. When the velocity profiles of the gas injectors were measured (fig. 4), an average curve was used, although a small variation was observed at different U_{max} and P_g. At different conditions ∇p and $2 \rho_g V^2/D_O$ may not be quite equal (eq. (2)) and thus cause spread in the data.

DISCUSSION

No measurements of the rate of liquid removal from a liquid jet during

the breakup process are presently available in the literature. This rate of breakup can be derived mathematically from the correlation of electrical resistance with distance (fig. 15). The results of this study can then be applied in calculating the rate at which the liquid mass reaches an atomized state.

The electrical resistance per unit length of liquid jet is inversely proportional to its cross-sectional area at any point along the jet. In figure 15, R/R_O is expressed as a function of distance or length, as represented by the average curve

$$\frac{R}{R_O} = 0.00392(3\epsilon_{av} - 1)^{3.34} + 1 \qquad \text{for} \quad \epsilon_{av} \geq 1/3$$

For a uniform velocity U over time t, the length-averaged distortion parameter $\epsilon_{av} = 1/3 \, \epsilon$ (see appendix), where ϵ is the distortion at a certain time t or distance L. Hence,

$$\frac{R}{R_O} = 0.00392(\epsilon - 1)^{3.34} + 1 \qquad \text{for} \quad \epsilon \geq 1$$

Since

$$R = \rho_E \int \frac{dL}{A} \quad \text{and} \quad R_O = \rho_E \frac{L}{A_O}$$

it follows that

$$\frac{R}{R_O} = \frac{1}{L} \int \frac{A_O}{A} \, dL$$

Differentiation gives

$$L \frac{d}{dL} \left(\frac{R}{R_O}\right) + \frac{R}{R_O} = \frac{A_O}{A}$$

Hence,

$$\frac{A}{A_O} = [0.00392(7.68\epsilon - 1)(\epsilon - 1)^{2.34} + 1]^{-1} \qquad \text{for} \quad \epsilon \geq 1$$

This equation is plotted in figure 17; the spread of data corresponding to that in figure 15 is also shown.

For all $\epsilon < 1$, figure 17 shows that no breakup should occur. This can be interpreted as the amount of distortion of the liquid cross section that must occur before any shredding of liquid from the edges begins. This breakup threshold is independent of the Weber number and should not be confused with the Weber threshold where surface forces balance the imposed dynamic forces.

13

Breakup is essentially complete for an ϵ value of 10 to 15. Designating this by ϵ_b, the time required for complete breakup can be found from equation (6):

$$t_b = \frac{D_o}{V} \sqrt{\epsilon_b \frac{\rho_l}{\rho_g}}$$

By differentiation again with respect to distance or time, the rate of area decrease, for $\epsilon \geq 1$, is

$$\frac{d}{dL}\left(\frac{A}{A_o}\right) = -0.00392 \left(\frac{A}{A_o}\right)^2 \left(\frac{2\epsilon}{L}\right)(25.65\epsilon - 10.02)(\epsilon - 1)^{1.34} \qquad (10)$$

or

$$\frac{d}{dt}\left(\frac{A}{A_o}\right) = -0.00392 \left(\frac{A}{A_o}\right)^2 \left(\frac{2\epsilon}{t}\right)(25.65\epsilon - 10.02)(\epsilon - 1)^{1.34} \qquad (11)$$

Hence, from the original measurements of electrical resistance as a function of ϵ_{av}, it is possible to derive expressions for the extent of breakup and rate of breakup as a function of time and environmental conditions. For convenience, let

$$\lambda_L = \frac{\rho_g}{\rho_l}\left(\frac{V}{v_l D_o}\right)^2 \quad \text{and} \quad \lambda_t = \frac{\rho_g}{\rho_l}\left(\frac{V}{D_o}\right)^2$$

so that

$$\lambda_L L^2 = \lambda_t t^2 = \epsilon$$

Figure 18 shows the variation of $\frac{d}{dL}\left(\frac{A}{A_o}\right)$ or $\frac{d}{dt}\left(\frac{A}{A_o}\right)$ with length L or time t, respectively, for several values of λ_L or λ_t, respectively. These curves should be considered very approximate in shape and amplitude since they depend on a particular choice of average curve in figure 15.

COMPARISON WITH OTHER EXPERIMENTAL RESULTS

A number of different studies have been made of the breakup of drops and jets in a gaseous stream. Suitable assumptions allow the results of the study herein to be compared with other data obtained under a wide diversity of conditions. The fact that reasonable agreement in the results exists is an indication of the generality of this approach.

Reference 15 describes drop size studies of the breakup of various fuels

injected into a crosscurrent air stream inside a tunnel. Included with this data was a relative mass-distribution survey made 1 inch downstream from the liquid injector centerline where breakup was complete. These data are plotted as part of figure 19. The conditions under which these data were obtained were quite different from the conditions for the present study: iso-octane has a specific gravity of 0.68 and a surface tension only 30 percent that of water; the orifice diameter was 0.030 inch and its length to diameter ratio was about 1; the test section was a 4- by 12-inch tunnel at a pressure slightly less than 1 atmosphere. The results of the present study may be applied to the experimental conditions of reference 15 to calculate the rate of breakup of the fuel jet; the disintegrated liquid would then be convected downstream by the flowing gas to the point where the mass-distribution measurements were made. The rate of breakup (mass released per unit distance) predicted by equation (10) of this study is shown to a relative scale along the fuel jet centerline. Drop trajectories for the maximum (D_{max}) and average (D_{30}) measured drop sizes are calculated and are shown for each run. These trajectories assume that no modification of the gas velocity is caused by the spray of liquid. At low gas velocities the effect of gas entrainment by the liquid spray is more severe, so that in runs 4 and 11 the trajectories shown would be displaced to larger values of x. Reasonable correspondence exists between the calculated mass distribution as it is convected downstream, and the measured distribution of reference 15.

Investigations of liquid jet breakup by a shock wave have demonstrated that the jet is broken by the gas flow behind the shock front. There the liquid experiences conditions similar to those of this study. In the shock-tube study of liquid jet breakup made in reference 17, the flow behind a shock wave moving transverse to the liquid jet caused disintegration to occur simultaneously at all points along its length. The time required for complete breakup to occur was judged visually from high-speed frame and streak photographs. The measured breakup times were compared with calculated times derived on the basis of two different models of the breakup process: (1) breakup controlled by the intermixing of liquid and gaseous boundary layers and (2) breakup controlled by the growth of surface oscillations to an unstable degree of distortion. Figure 20 compares the measured breakup times of reference 17 with those calculated from 99-percent breakup $(A/A_O = 0.01)$ on the basis of the present study. These times show somewhat better accord with the measured times than the calculated times of reference 17. Some of the scatter in data is introduced in the visual judgement of the point of breakup in determining measured breakup times. A subsequent study (ref. 18) measured breakup times of jets of various liquids.

As a liquid cylinder flattens in one direction transverse to a flow of gas, a sphere should flatten in two directions forming a disk, since similar external pressure profiles exist. Photographs of the breakup of water drops in a shock tube from reference 35 show the beginning of disk formation before tangential forces tear off the thin periphery. Figures 4 and 9 to 12 of reference 35 show breakup commencing at time and conditions giving a calculated value of $\epsilon \approx 0.5$, and complete breakup at $\epsilon \approx 10$ to 15. The rate of flattening calculated on the basis of this study is equal to that shown at lower shock strengths, but considerably less than the flattening shown for a 1.7 Mach number shock. Equation (31) in reference 35 is similar to distortion equation (6), but in computing the distortion rate the total pressure is inserted

rather than the differential in pressure around the drop.

Similar drop breakup studies in references 29, 34, and 36 show breakup starting at calculated ϵ values of 1 to 2, and generally completed at about 10 to 15, or as high as 20 to 30 estimated for the data of reference 29. The aforementioned references include drop breakup pictures for 230- to 4000-micron diameter drops of water, methyl alcohol, and burning and nonburning hydrocarbon fuels. Gas velocities ranged from 60 to 1450 feet per second. It is important to note that in each of these references including reference 35, considerable distortion of the liquid cross section occurs before appreciable stripping off of liquid drops takes place.

Distortion rates of drops being accelerated through gas nozzles in experiments described in reference 27 are considerably lower than predicted by this study; however, the surface forces should be expected to stabilize the drops, since the Weber numbers were only of the order of 5 to 10 or less.

In the series of reports on liquid atomization of reference 16 pictures and drop sizes of breakup in a crossflow of gas are shown. At the low liquid velocities reported therein, breakup should occur in one to two jet diameters of jet length, which the photographs in reference 16 seem to indicate.

Thus, it appears that in a wide variety of cases, both liquid cylinders and liquid spheres can be considered to offer only inertial resistance to distorting forces resulting from a crosscurrent flow of gas. The breakup rates measured electrically in this study can be applied to those other breakup situations provided that the Weber numbers are well above their threshold for breakup.

A number of analytical expressions have been proposed for the rate or time required for a liquid jet to break up or atomize. These were derived on the basis of each proposed model or explanation of the mechanism of breakup. The importance of the various parameters in these expressions reflects the forces and effects considered important in each reference. The exponents on the various parameters of which breakup time is an exponential function are listed in the following table. For example, in the present study,

$$t_b \propto \frac{D_o}{V} \sqrt{\frac{\rho_l}{\rho_g}}$$

In several cases, the variables do not appear as pure exponentials, but for purposes of comparison they have been approximated as such in the table. Models for injection of liquid into stagnant gas as well as crosscurrent flow of gas are included.

Source	Gas flow	Liquid drop or jet diameter	Relative velocity of the gas with respect to the liquid, V	Liquid density, ρ_l	Gas density, ρ_g	Surface tension, σ	Liquid viscosity, μ_l	Gas viscosity, μ_g
Present study	Cross-current	1	-1	1/2	-1/2	(a)	(a)	(a)
Reference 30[b]	Cross-current	1	-1	1/2	-1/2	(a)	(a)	(a)
Reference 31	Stagnant	1	-1	1/2	-1/2	(a)	(a)	(a)
Reference 17[c]	Cross-current	1 to 5/4	-1/2 to -1/4	1/2	-1/2 to -1/4	-1/2	(a)	1/2 to 1/4
Reference 17[d]	Cross-current	5/4	-5/4	2/3	-5/12	1/2	-1/3	-5/12
Reference 18	Cross-current	1.5 to 1.12	-0.5 to -1.05	0.67 to 0.6	-0.17 to -0.48	0 to 0.17	-0.33 to -0.26	-0.17 to -0.03
Reference 33	Stagnant	3/2	(a)	1/2	(a)	-1/2	(a)	(a)
Reference 43	Stagnant	3/2 to 1	(a)	1/2 to 0	(a)	-1/2 to -1	0 to 1	(a)

[a]Effects neglected by author or for purpose of this comparison.

[b]For low σ and μ_l.

[c]For $We \gg Re$, deformation model.

[d]For $We \gg Re$, boundary-layer model.

CONCLUSIONS

Photographs of the breakup zone of a water jet in a transverse flow of nitrogen gas show the increase in breakup with increasing gas velocity and density and action distance and with decreasing liquid jet diameter and velocity. The average total resistance of the jet along its length increases sharply with increasing breakup. A correlation has been found experimentally between the electrical resistance and the factors affecting the breakup.

A successful model of liquid jet breakup in a crossflow of gas at high Weber numbers consists of a progressive liquid spreading transverse to the gas flow in response to the pressure distribution at the liquid surface and resisted only by the inertia of the liquid. The degree of breakup is reasonably correlated as a function of the degree of spreading ϵ, where.

$$\epsilon = \frac{\delta}{D_o} = \frac{\rho_g}{\rho_l}\left(\frac{VL}{v_l D_o}\right)^2 = \frac{\rho_g}{\rho_l}\left(\frac{Vt}{D_o}\right)^2$$

Photographs corroborate the fact that liquid spreading takes place transverse to the gas flow. Breakup starts at an ϵ of 1 or 2 or at a time of

$$t_i = \frac{D_o}{V}\sqrt{(1 \text{ or } 2)\frac{\rho_l}{\rho_g}};$$ it is essentially complete at $\epsilon = 10$ to 15, or time

$$t_b = \frac{D_o}{V}\sqrt{(10 \text{ to } 15)\frac{\rho_l}{\rho_g}}.$$

The electrical resistance along the length of a liquid jet appears to be a good measure of jet breakup. It is inversely proportional to the average along the jet length of the cross-sectional area. The resistance is much more sensitive to environmental changes than visual criteria and is less prone to subjective errors. Time averaging of the high-frequency fluctuations in degree of breakup is simple and convenient with an electrical signal but difficult visually.

Other breakup data for both liquid jets and liquid drops are fairly well correlated by the suggested breakup criterion ϵ. These data include liquids of lower density and lower surface tension than water and gas velocities generated behind a shock wave and in a tunnel.

It is suggested that this breakup criterion may be applicable also to the breakup of conventional fuels or cryogenic oxidants in a rocket engine when transverse velocities exist.

Lewis Research Center
    National Aeronautics and Space Administration
        Cleveland, Ohio, February 25, 1964

APPENDIX - DERIVATION OF CORRECTION FACTOR N FOR

AVERAGE DISTORTION WITH NONUNIFORM GAS VELOCITY

In the integrations of equations (3) to (5) to find the liquid displacement δ, it was assumed that the gas velocity U was constant with time. In the experimental equipment, however, U was a function of position with respect to the gas injector. Hence, in deriving the expression for ϵ to be used in correlating the experimental data, U must be considered a variable in each integration step. The distortion ϵ can be calculated from the maximum value of the gas velocity U_{max} and a correction factor as follows:

$$a = 2 \frac{\rho_g}{\rho_l} \frac{V^2}{D_o}$$

where $V^2 = U^2 + v_l^2$ and $U = U(t)$, or

$$a = 2 \frac{\rho_g}{\rho_l} \left(\frac{V_{max}}{D_o}\right)^2 \left(\frac{V}{V_{max}}\right)^2$$

$$w = 2 \frac{\rho_g}{\rho_l} \left(\frac{V_{max}}{D_o}\right)^2 \int_0^t \left(\frac{V}{V_{max}}\right)^2 dt$$

$$\epsilon = \frac{\delta}{D_o} = 2 \frac{\rho_g}{\rho_l} \left(\frac{V_{max}}{D_o}\right)^2 \int_0^t \int_0^t \left(\frac{V}{V_{max}}\right)^2 dt \, dt$$

or

$$\epsilon = 2 \frac{\rho_g}{\rho_l} \left(\frac{V_{max}}{v_l D_o}\right)^2 \int_0^L \int_0^x \left(\frac{V}{V_{max}}\right)^2 dx \, dx \qquad (A1)$$

Normalizing the distance by the total distance yields

$$\epsilon = 2 \frac{\rho_g}{\rho_l} \left(\frac{V_{max} L}{v_l D_o}\right)^2 \int_0^1 \int_0^\xi \left(\frac{V}{V_{max}}\right)^2 d\xi \, d\xi$$

The correction factor to ϵ calculated using V_{max} is then

$$2 \int_0^1 \int_0^\xi \left(\frac{V}{V_{max}}\right)^2 d\xi \, d\xi$$

When U is constant with distance or time, $V = V_{max}$ and the correction factor reduces to unity.

The relative distortion ϵ and hence the degree of liquid breakup is then a function of L and a correction factor calculated to that point in the liquid jet. However, the electrical resistance is a function of the average degree of breakup over the length of the jet; the resistance is then a function of a length average of ϵ and is so graphically correlated.

$$\epsilon_{av} = \frac{1}{L} \int_0^L \epsilon \, dx = \int_0^1 \epsilon \, d\xi$$

$$= 2 \frac{\rho_g}{\rho_l} \left(\frac{V_{max} L}{v_l D_o}\right)^2 \int_0^1 \int_0^\xi \int_0^\xi \left(\frac{V}{V_{max}}\right)^2 d\xi \, d\xi \, d\xi$$

$$= N \frac{\rho_g}{\rho_l} \left(\frac{V_{max} L}{v_l D_o}\right)^2 \tag{A2}$$

where

$$N = 2 \int_0^1 \int_0^\xi \int_0^\xi \left(\frac{V}{V_{max}}\right)^2 (d\xi)^3 \tag{A3}$$

When U is constant, N reduces to $1/3$.

REFERENCES

1. Priem, Richard J., and Heidmann, Marcus F.: Propellant Vaporization as a Design Criterion for Rocket-Engine Combustion Chambers. NASA TR-67, 1960.

2. Dityakin, I. F., and Yagodkin, V. I.: Effect of Periodic Oscillations of Velocity and Density of a Medium on Disintegration of Liquid Jets. NASA TT F-63, 1961.

3. Sitkei, Gyorgy: Contribution to the Theory of Jet Atomization. NASA TT F-129, 1963.

4. Clark, Bruce J.: Propellant Vaporization as a Criterion for Rocket-Engine Design: Experimental Effect of Combustor Length, Throat Diameter, Injection Velocity, and Pressure on Rocket Combustor Efficiency. NASA TN D-258, 1960.

5. Pilcher, J. M., and Miesse, C. C.: The Mechanism of Atomization. Injection and Combustion of Liquid Fuels, ch. I, TR 56-344, WADC, Mar. 1957, pp. 1-1 - 1-57.

6. Priem, Richard J., and Morrell, Gerald: Application of Similarity Parameters for Correlating High-Frequency Instability Behavior of Liquid Propellant Combustors. Paper 1721-61, Am. Rocket Soc., Inc., 1961.

7. Bertschy, A. W., Armington, A. F., Moran, H. E., and Tuve, R. L.: A Portable Water-Spray Fire Extinguisher for Submarine Use. Rep. 4363, Naval Res. Lab., June 8, 1954.

8. Rasbash, D. J.: The Properties of Sprays Produced by Batteries of Impinging Jets. F. R. Note 181/1955, Dept. Sci. and Ind. Res. and Fire Offices' Comm. Joint Fire Res. Organization, Boreham Wood (England), May 1955. (Abs. in Spray Literature Abs., K. G. DeJuhasz, ed., ASME, 1959, p. 287.)

9. Euteneuer, G. A.: Druckabhängigkeit von Tropfengrösse und Wurfweite bei Sprühstrahlen. (Drop Size and Throw Distance of Jet Sprays as Functions of Pressure.) VFDB Zs., bd. 6, no. 3, Aug. 1957, pp. 124-128. (Abs. in Appl. Mech. Rev., vol. 11, 1958, p. 578.)

10. Kumano, Y., and Ishizaka, K.: An Experimental Study on the Solidity of Extinguisher Stream. Quarterly Rep. of Fire Res. Inst. (Japan), vol. 3, no. 3, Dec. 1952, pp. 88-93; vol. 3, no. 4, Mar. 1953, pp. 114-124. (Abs. in Spray Literature Abs., K. J. DeJuhasz, ed., ASME, 1959, p. 190.)

11. Giffen, Edmund, and Muraszew, A.: The Atomisation of Liquid Fuels. John Wiley & Sons, Inc., 1953.

12. Schweitzer, P. H.: Penetration of Oil Sprays. Bull. Penn. State College, 46, 1937.

13. Biles, Martin B.: An Analysis of Short Length Liquid Sprays. Heat Transfer and Fluid Mech. Inst., ASME, 1949, pp. 41-50.

14. Debeauvais, F.: Quelques Aspects de la Desagregation des Jets Liquides dans l'Air en Mouvement. IXth Congrés International de Mécanique Appliquée, Tome I, 1957.

15. Ingebo, Robert D., and Foster, Hampton H.: Drop-Size Distribution for Crosscurrent Breakup of Liquid Jets in Airstreams. NACA TN 4087, 1957.

16. Nukiyama, S., and Tanasawa, Y.: Experiments on the Atomization of Liquids in an Air Stream. Rep. 6, Trans. from Soc. Mech. Eng. (Japan), vol. 6, no. 23, May 1940, p. 11. (Trans. Defense Res. Board (Canada), Mar. 18, 1950.)

17. Morrell, Gerald: Rate of Liquid Jet Breakup by a Transverse Shock Wave. NASA TN D-1728, 1963.

18. Morrell, Gerald, and Povinelli, F. P.: Breakup of Various Liquid Jets by Shock Waves. NASA TP 3-63, 1963.

19. Muirhead, J. C.: Blast Wave Attenuation. Pt. 1. Water Walls. TP-175, Suffield Experimental Station (Canada), 1959.

20. Degtev, O. N.: Deformation of Drops in a Flow of Gas and the Drops' Stability Limit. (In Russian.) Trudi Ural'skogo Politekhn. In-ta, no. 61, 1956, pp. 106-112. (Abs. from Appl. Mech. Rev., vol. 12, 1959, p. 730.)

21. Hinze, J. O.: Forced Deformations of Viscous Liquid Globules. Appl. Sci. Res., vol. A1, 1949, pp. 263-272.

22. Hinze, J. O.: Critical Speeds and Sizes of Liquid Globules. Appl. Sci. Res., vol. A1, 1949, pp. 273-288.

23. Hrubecky, Henry F.: Experiments in Liquid Atomization by Air Streams. Jour. Appl. Phys., vol. 29, no. 3, Mar. 1958, pp. 572-578.

24. Weiss, Malcolm A., and Worsham, Charles H.: Atomization in High Velocity Airstreams. ARS Jour., vol. 29, no. 4, Apr. 1959, pp. 252-259.

25. Buchmann, S. W.: An Experimental Investigation of Drop Disintegration. (In Russian.) Akad. Nauk Kaz. SSR, ALMA-ATA Vestnik, vol. 11, 1955, pp. 80-87.

26. Lane, W. R.: Shatter of Drops in Streams of Air. Ind. and Eng. Chem., vol. 43, no. 6, June 1951, pp. 1312-1317.

27. Isshiki, Naotsugu: Theoretical and Experimental Study on Atomization of a Liquid Drop in High Speed Gas Stream. Rep. 35, Transportation Tech. Res. Inst. (Japan), July 1959. (See also Paper 355-56, American Rocket Soc., Inc., 1956.)

28. Volynskiy, M. S.: On the Break-up of Droplets in an Airstream. Akad. Nauk., USSR, Doklady, vol. 62, 1948, pp. 301-304.

29. Wilcox, James D., and June, Ronald K.: Apparatus for Study of the Breakup of Liquid Drops by High Velocity Airstreams. Jour. Franklin Inst., vol. 271, no. 3, Mar. 1961, pp. 169-183.

30. Gordon, G. D.: Mechanism and Speed of Breakup of Drops. Jour. Appl. Phys., vol. 30, no. 11, Nov. 1959, pp. 1759-1761.

31. Siestrunck, M. Raymond: Sur les Régimes de Résolution des Jets Liquides sous l'Influence d'un Soufflage Axial. Academie des Sciences, Comptes Rendux, vol. 215, July 1942, pp. 404-406.

32. Dodd, K. N.: On the Disintegration of Water Drops by Shock Waves. TN MS 64, British RAE, May 1960.

33. Baron, Thomas: Atomization of Liquid Jets and Droplets. TR-4, Univ. Ill., Feb. 15, 1949.

34. Hanson, A. R., Domich, E. G., and Adams, H. S.: An Experimental Investigation of Impact and Shock-Wave Break-Up of Liquid Drops. Res. Rep. 125, Rosemount Aero. Lab., Jan. 1956.

35. Engel, Olive G.: Fragmentation of Waterdrops in the Zone Behind an Air Shock. NBS Jour. of Res., Res. Paper 2843, vol. 60, no. 3, Mar. 1958, pp. 245-280.

36. Rabin, E., and Lawhead, R.: The Motion and Shattering of Burning and Non-burning Propellant Droplets. TN-59-129, Office Sci. Res., Mar. 25, 1959.

37. Panasenkov, N. S.: The Effect of Turbulence of a Liquid Jet on Its Dispersion. Zhurnal Tekh. Fiz., vol. 21, no. 2, Feb. 1951, pp. 160-166.

38. Koros, R. M., Deckers, J. M., and Boudart, M. J.: Observations on Liquid Sheets Formed by Colliding Vertical Jets. TN 60-234, Office Sci. Res., 1960.

39. Goldstein, Sydney: Modern Developments in Fluid Dynamics. Clarendon Press (Oxford), 1938.

40. Roshko, Anatol: Experiments on the Flow Past a Circular Cylinder at Very High Reynolds Number. Jour. Fluid Mech., vol. 10, no. 3, May 1961, pp. 345-356.

41. Sykes, D. M.: The Supersonic and Low-Speed Flows Past Circular Cylinders of Finite Length Supported at One End. Jour. Fluid Mech., vol. 12, no. 3, Mar. 1962, pp. 367-387.

42. Sogin, H. H., and Subramanian, V. S.: Local Mass Transfer from Circular Cylinders in Cross Flow. Jour. Heat Transfer (Trans. ASME), ser. C, vol. 83, no. 4, Nov. 1961, pp. 483-493.

43. Schweitzer, P. H.: Mechanism of Disintegration of Liquid Jets. Jour. Appl. Phys., vol. 8, no. 8, Aug. 1937, pp. 513-521.

24
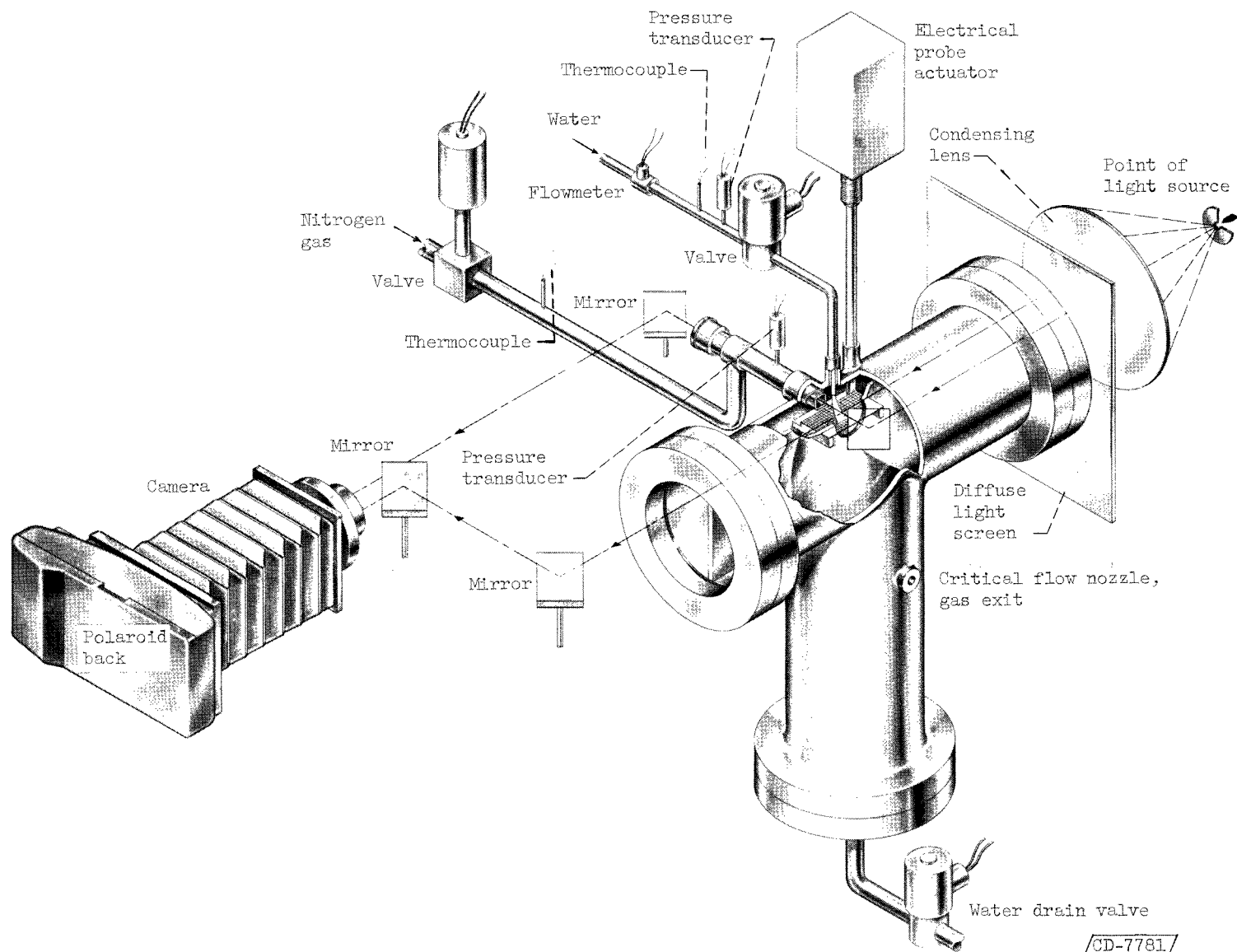
Figure 1. - Spray test chamber and optical system.
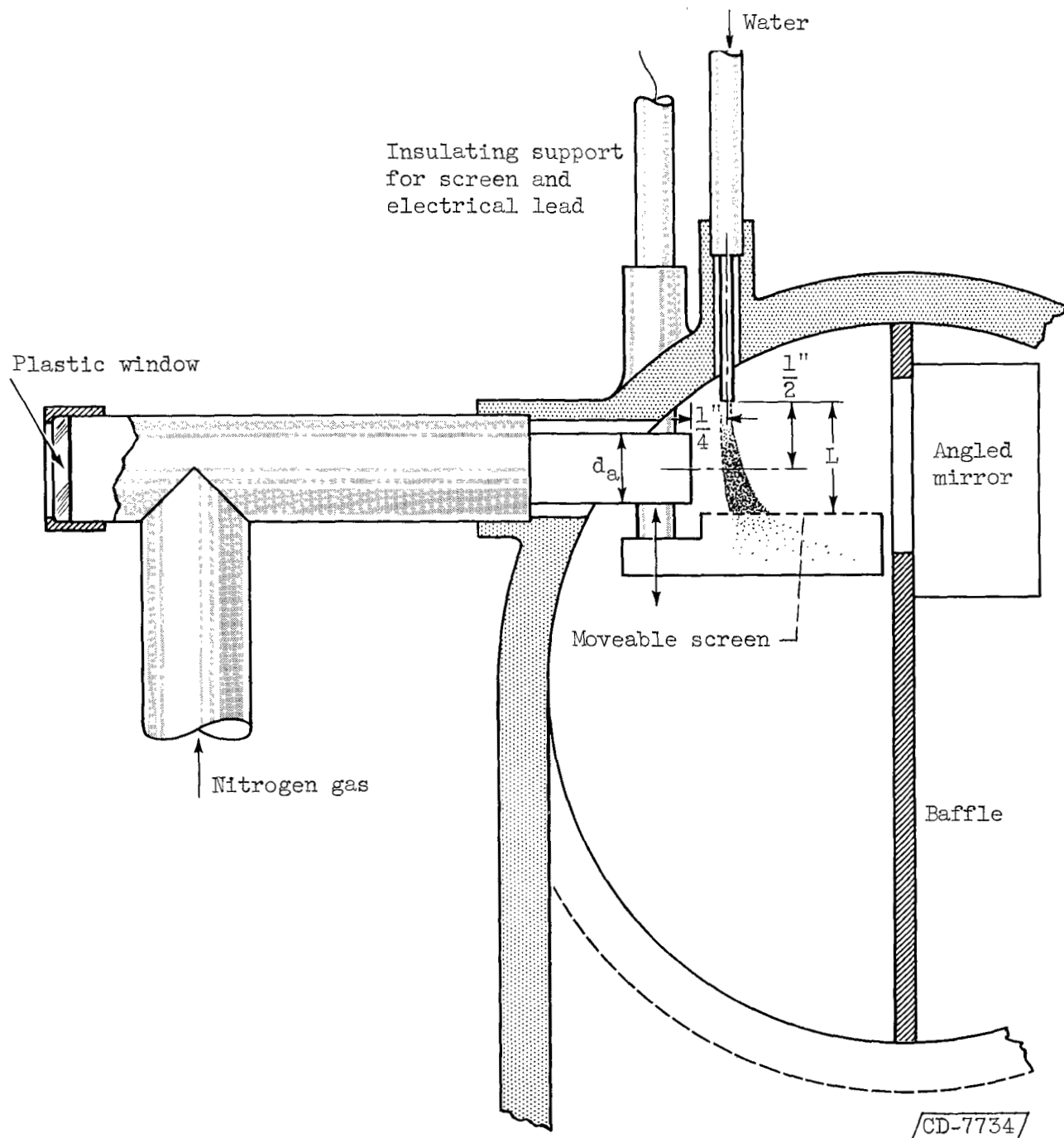
Figure 2. - Geometry of stream impingement.
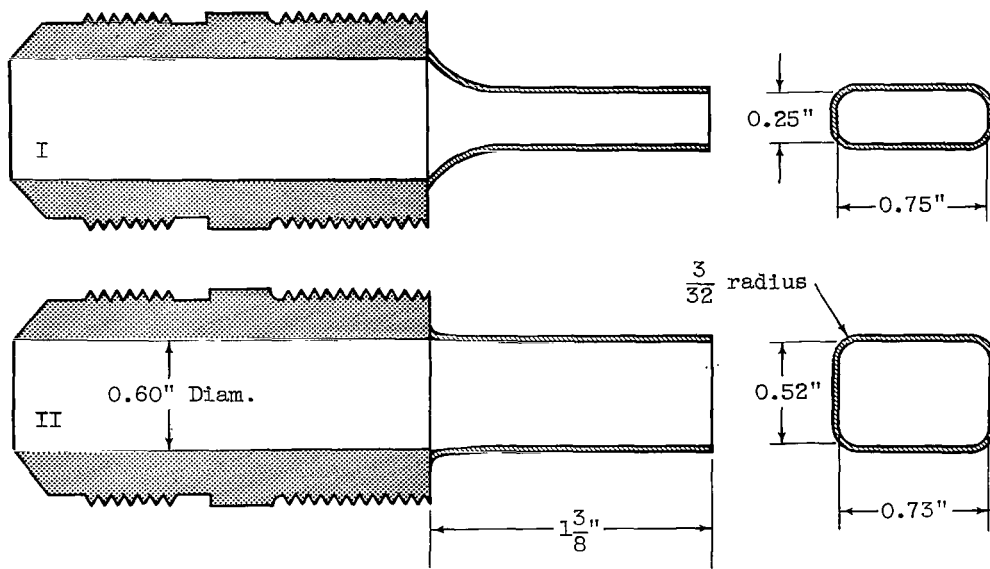
(a) Gas injectors.
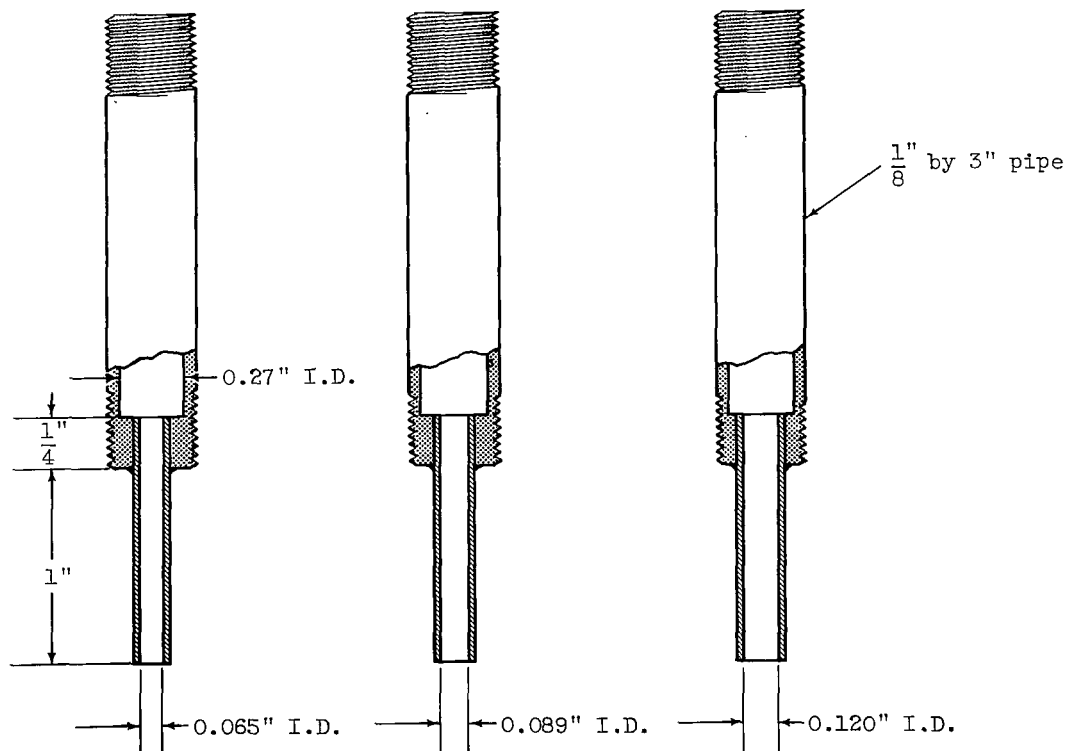
(b) Liquid injectors.

Figure 3. - Injector details, showing interior dimensions.
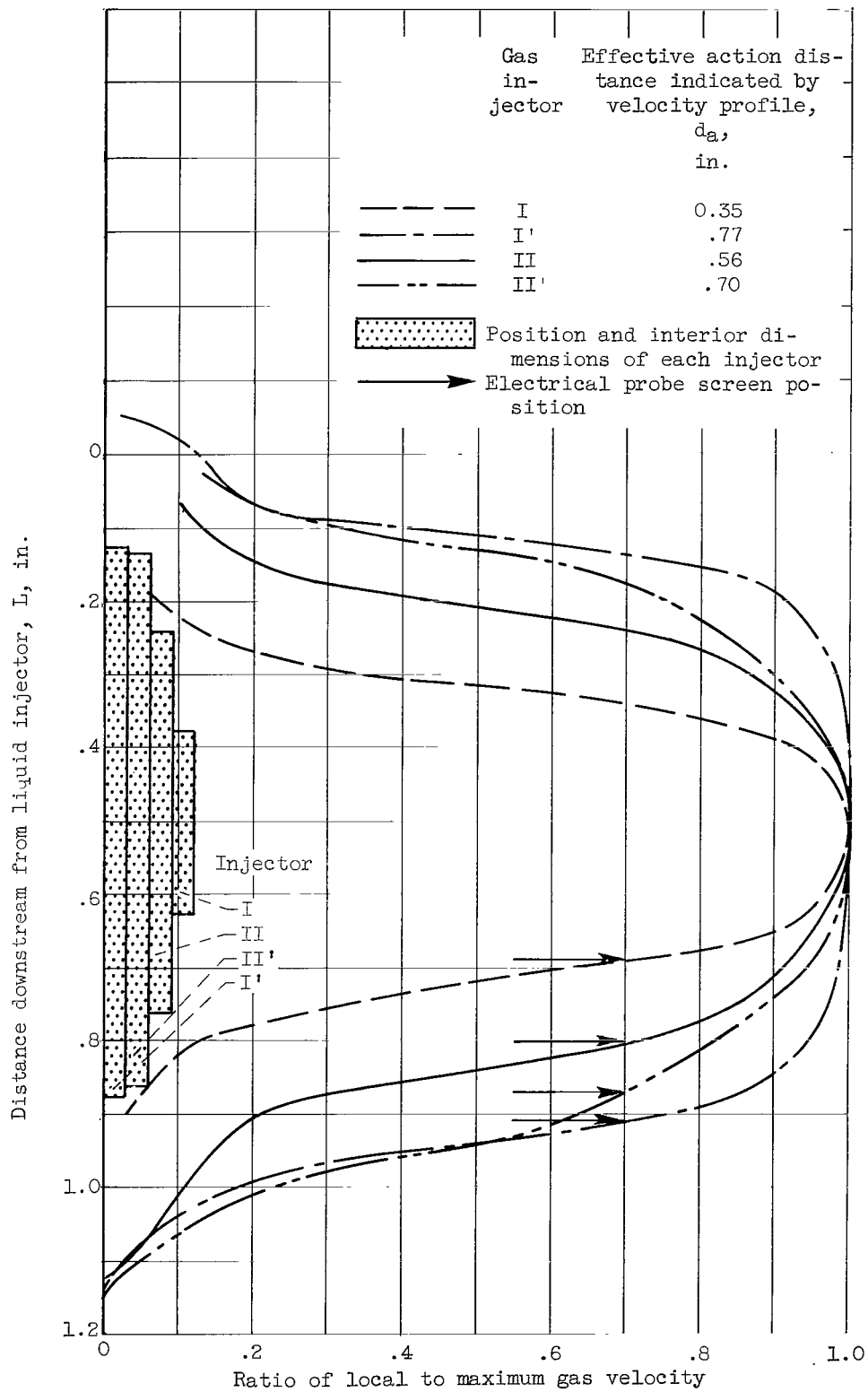
Figure 4. - Velocity profiles of gas injectors.
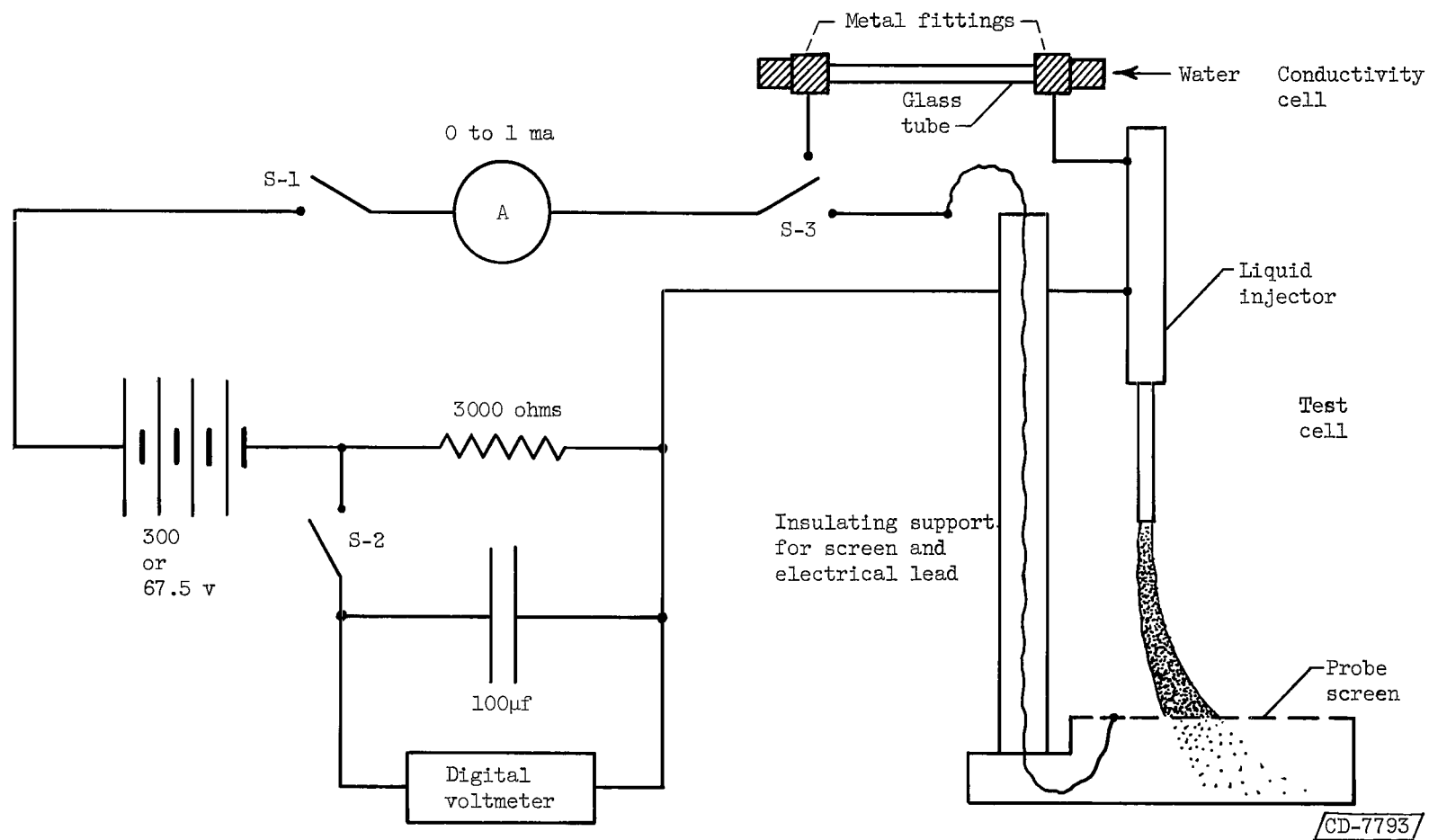
Figure 5. - Electrical circuit for spray-resistance and water-conductivity measurements.
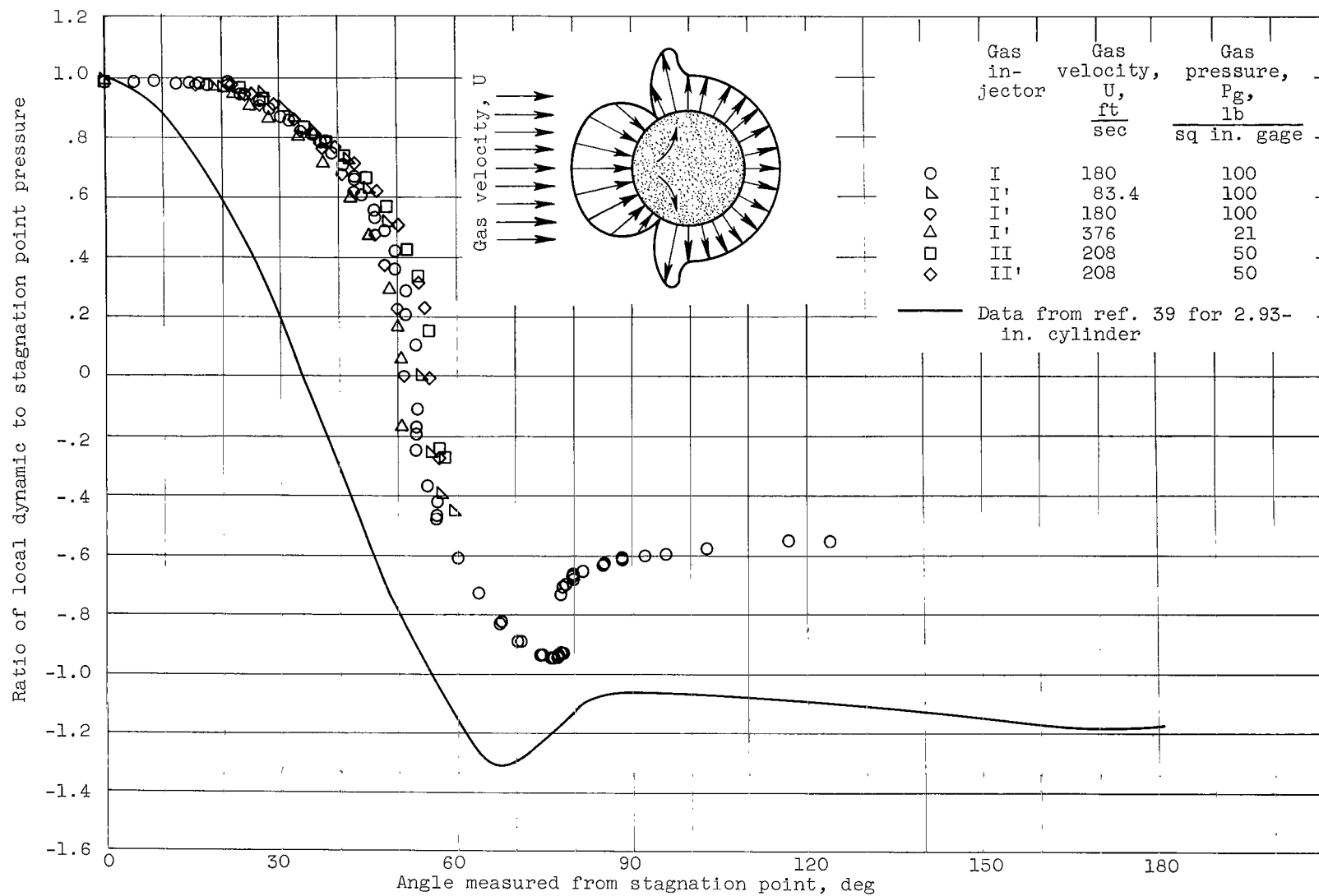
Figure 6. - Dynamic pressure distribution around cylinder. Measured data for 1/8-inch cylinder with different gas injectors are compared with data of reference 39.
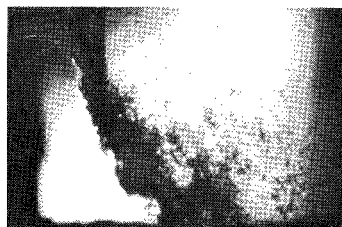
Axial velocity of liquid jet v_l = 19 ft/sec v_l = 48.8 ft/sec
Length average of liquid
     distortion ϵ_{av} = 3.36 ϵ_{av} = 0.591
Ratio of measured to
     undistorted resistance R/R_0 = 10.3 R/R_0 = 1.62

v_l = 23.4 ft/sec v_l = 62.4 ft/sec
ϵ_{av} = 2.26 ϵ_{av} = 0.405
R/R_0 = 3.68 R/R_0 = 1.49
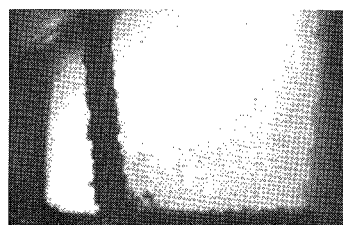
C-68960

v_l = 38.8 ft/sec
ϵ_{av} = 0.875
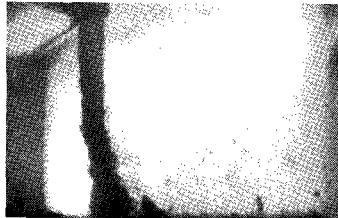R/R_0 = 1.63

Figure 7. - Effect of liquid velocity alone upon breakup showing correlation with
    electrical resistance. Orifice diameter, 0.089 inch; orifice length to diameter
    ratio, 100; gas velocity, 127.5 feet per second; gas pressure, 40 pounds per
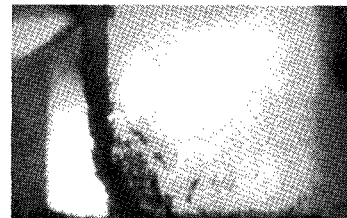   square inch gage; gas injector, II.
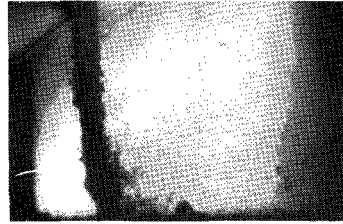
Pressure in gas phase $P_g = 40$ lb/sq in. gage $P_g = 150$ lb/sq in. gage
Length average of liquid
     distortion $\epsilon_{av} = 0.616$ $\epsilon_{av} = 1.80$
Ratio of measured to
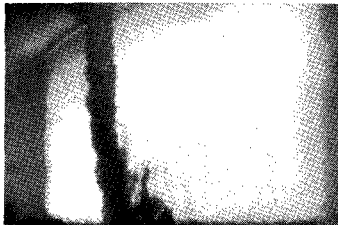   undistorted resistance $R/R_0 = 1.48$ $R/R_0 = 2.61$
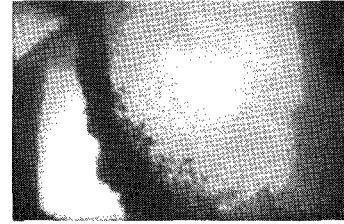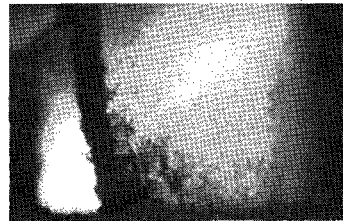
$P_g = 71$ lb/sq in. gage $P_g = 200$ lb/sq in. gage
$\epsilon_{av} = 0.952$ $\epsilon_{av} = 2.40$
$R/R_0 = 1.61$ $R/R_0 = 3.58$
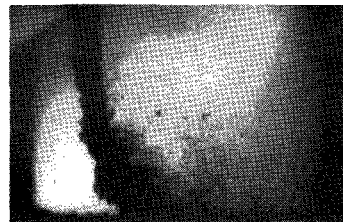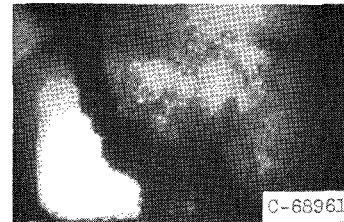
$P_g = 101$ lb/sq in. gage $P_g = 249$ lb/sq in. gage
$\epsilon_{av} = 1.20$ $\epsilon_{av} = 2.85$
$R/R_0 = 1.85$ $R/R_0 = 4.54$

Figure 8. - Effect of gas pressure upon breakup showing correlation with electrical resistance. Orifice diameter, 0.089 inch; orifice length to diameter ratio, 100; liquid velocity, 47.7 to 50.1 feet per second; gas velocity, 127.2 feet per second; gas injector, II.
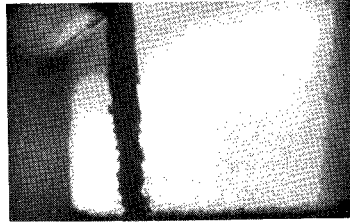
Gas velocity

Length average of
  liquid distortion

Ratio of measured to
  undistorted resistance

U = 66.5 ft/sec

ϵ_{av} = 0.246

R/R_0 = 1.18
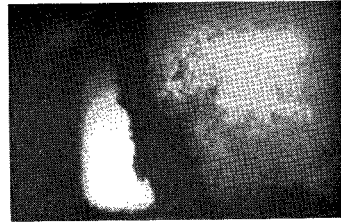
U = 210 ft/sec

ϵ_{av} = 1.44

R/R_0 = 1.68
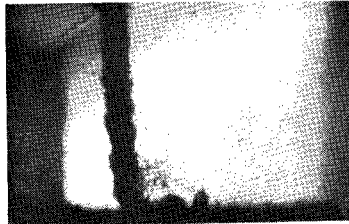
U = 99.8 ft/sec
ϵ_{av} = 0.425
R/R_0 = 1.21
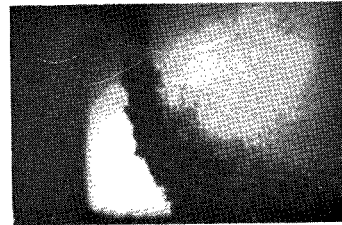
U = 247 ft/sec
ϵ_{av} = 1.99
R/R_0 = 2.71

U = 127.2 ft/sec
ϵ_{av} = 0.600
R/R_0 = 1.23
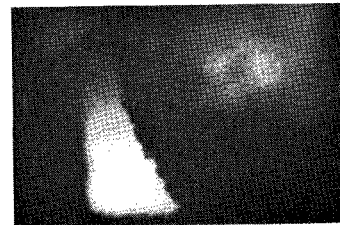
U = 314 ft/sec
ϵ_{av} = 3.12
R/R_0 = 7.70
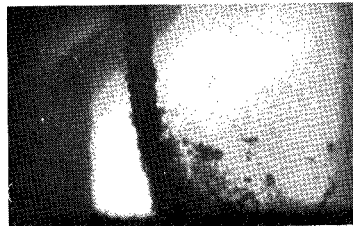
C-68962

U = 156.8 ft/sec
ϵ_{av} = 0.820
R/R_0 = 1.32

Figure 9. - Effect of gas velocity upon breakup showing correlation with electrical
  resistance. Orifice diameter, 0.089 inch; orifice length to diameter ratio, 100;
  liquid velocity, 48 to 49.5 feet per second; gas pressure, 40 pounds per square
  inch gage; gas injector, II.

33

Liquid jet diameter
Orifice length to diameter
  ratio
Length average of liquid
  distortion
Ratio of measured to
  undistorted resistance

$D_O = 0.065$ in.

$L_O/D_O = 19$

$\epsilon_{av} = 1.05$

$R/R_O = 1.41$

$D_O = 0.065$ in.

$L_O/D_O = 19$

$\epsilon_{av} = 1.82$

$R/R_O = 1.98$

$D_O = 0.089$ in.
$L_O/D_O = 14$
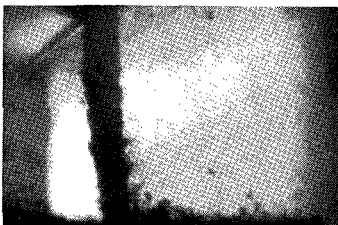$\epsilon_{av} = 0.600$
$R/R_O = 1.06$

$D_O = 0.089$ in.
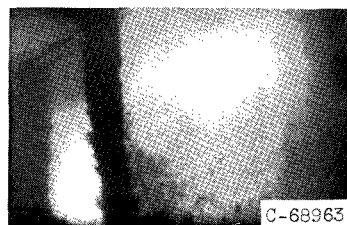$L_O/D_O = 14$
$\epsilon_{av} = 0.949$
$R/R_O = 1.13$

$D_O = 0.089$ in.
$L_O/D_O = 100$
$\epsilon_{av} = 0.599$
$R/R_O = 1.29$

$D_O = 0.089$ in.
$L_O/D_O = 100$
$\epsilon_{av} = 0.929$
$R/R_O = 1.24$

$D_O = 0.120$ in.
$L_O/D_O = 10.4$
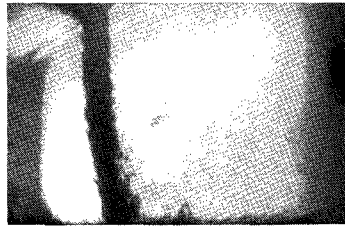$\epsilon_{av} = 0.346$
$R/R_O = 1.36$

$D_O = 0.120$ in.
$L_O/D_O = 10.4$
$\epsilon_{av} = 0.488$
$R/R_O = 1.27$

(a) Gas pressure, 39 to 42 pounds   (b) Gas pressure, 70 to 71 pounds
    per square inch gage.   per square inch gage.

Figure 10. - Effect of liquid jet diameter and orifice length to diameter ratio on breakup at two gas pressures. Liquid velocity, 46.7 to 51 feet per second; gas velocity, 126.6 to 127.6 feet per second; gas injector, II.
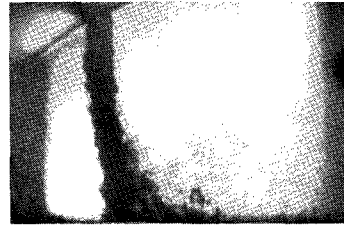
34

Gas injector   II ($d_a \approx 0.56$ in.)   II ($d_a \approx 0.56$ in.)

Length average of liquid
  distortion $\epsilon_{av} = 0.575$ $\epsilon_{av} = 0.940$

Ratio of measured to undistorted
  resistance $R/R_0 = 1.17$ $R/R_0 = 1.23$
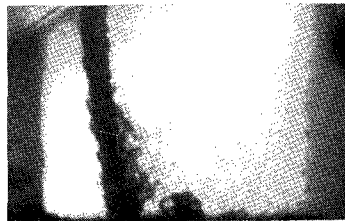
II' ($d_a \approx 0.704$ in.)   II' ($d_a \approx 0.704$ in.)

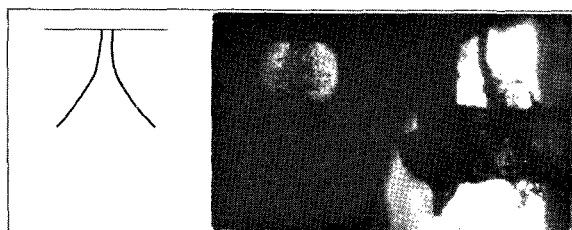$\epsilon_{av} = 0.833$ $\epsilon_{av} = 1.25$

$R/R_0 = 1.27$ $R/R_0 = 1.45$
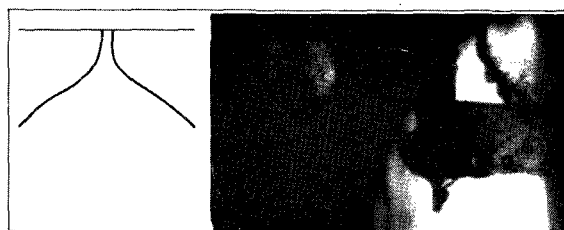
(a) Gas pressure, 39 to 40 pounds   (b) Gas pressure, 69 to 70 pounds
      per square inch gage.   per square inch gage.

Figure 11. - Effect of action distance d_a on breakup at two gas pressures. Orifice
diameter, 0.089 inch; orifice length to diameter ratio, 100; liquid velocity, 48 to
49.5 feet per second; gas velocity, 127.2 feet per second.

Axial velocity of liquid jet v_l = 31.9 ft/sec
Length average of liquid
 distortion ϵ_{av} = 1.246
Ratio of measured to undistorted
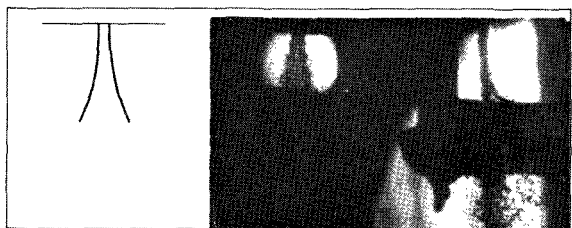 resistance R/R_0 = 1.40

v_l = 31.2 ft/sec
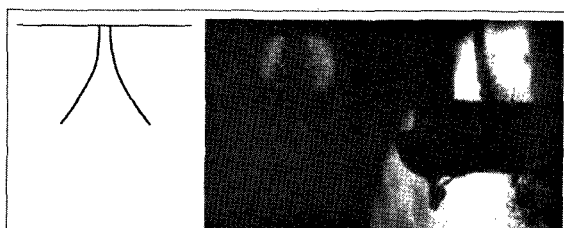ϵ_{av} = 2.75
R/R_0 = 8.62
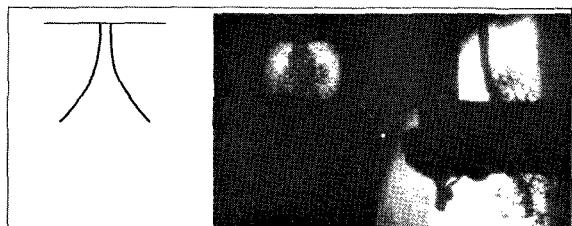
v_l = 37 ft/sec
ϵ_{av} = 0.956
R/R_0 = 1.35

v_l = 37.7 ft/sec
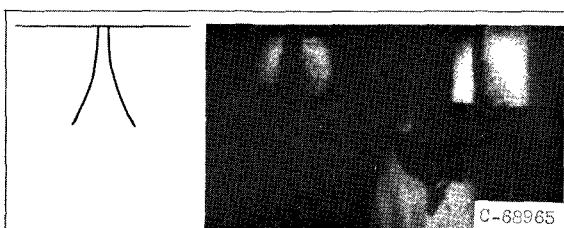ϵ_{av} = 1.936
R/R_0 = 2.39

v_l = 56.3 ft/sec
ϵ_{av} = 0.470
R/R_0 = 1.15

v_l = 55.6 ft/sec
ϵ_{av} = 1.012
R/R_0 = 1.25

v_l = 72.4 ft/sec
ϵ_{av} = 0.326
R/R_0 = 1.08

v_l = 81.4 ft/sec
ϵ_{av} = 0.595
R/R_0 = 1.10

(a) Gas pressure, 40 pounds per square inch gage.   (b) Gas pressure, 101 to 102 pounds per square inch gage.

Figure 12. - Perpendicular views of jet breakup showing effects of jet velocity and gas pressure on spreading of jet transverse to gas stream. Patterns of calculated rate of spreading are shown for each case. Orifice diameter, 0.089 inch; orifice length to diameter ratio, 100; gas velocity, 126.7 to 127.5 feet per second; gas injector, II.

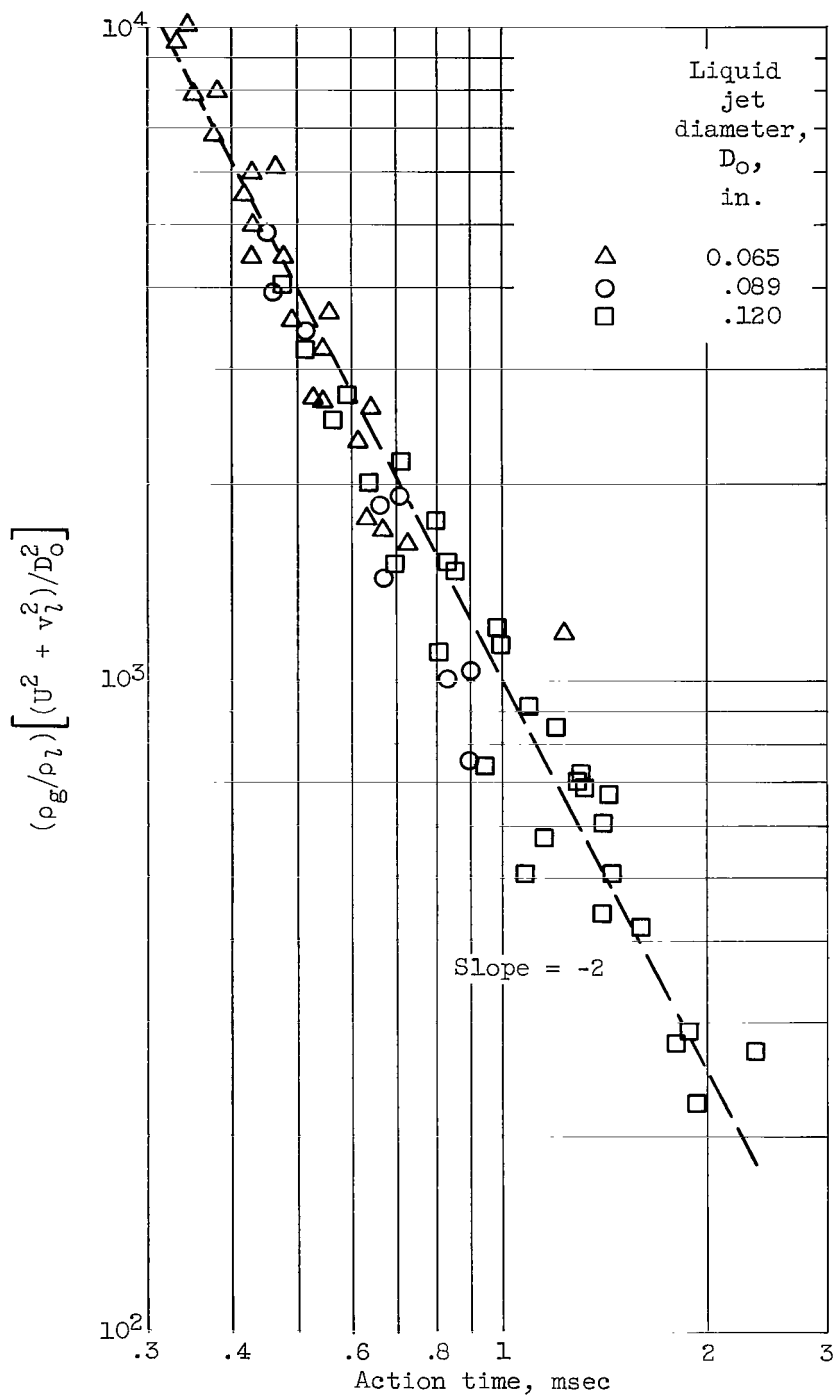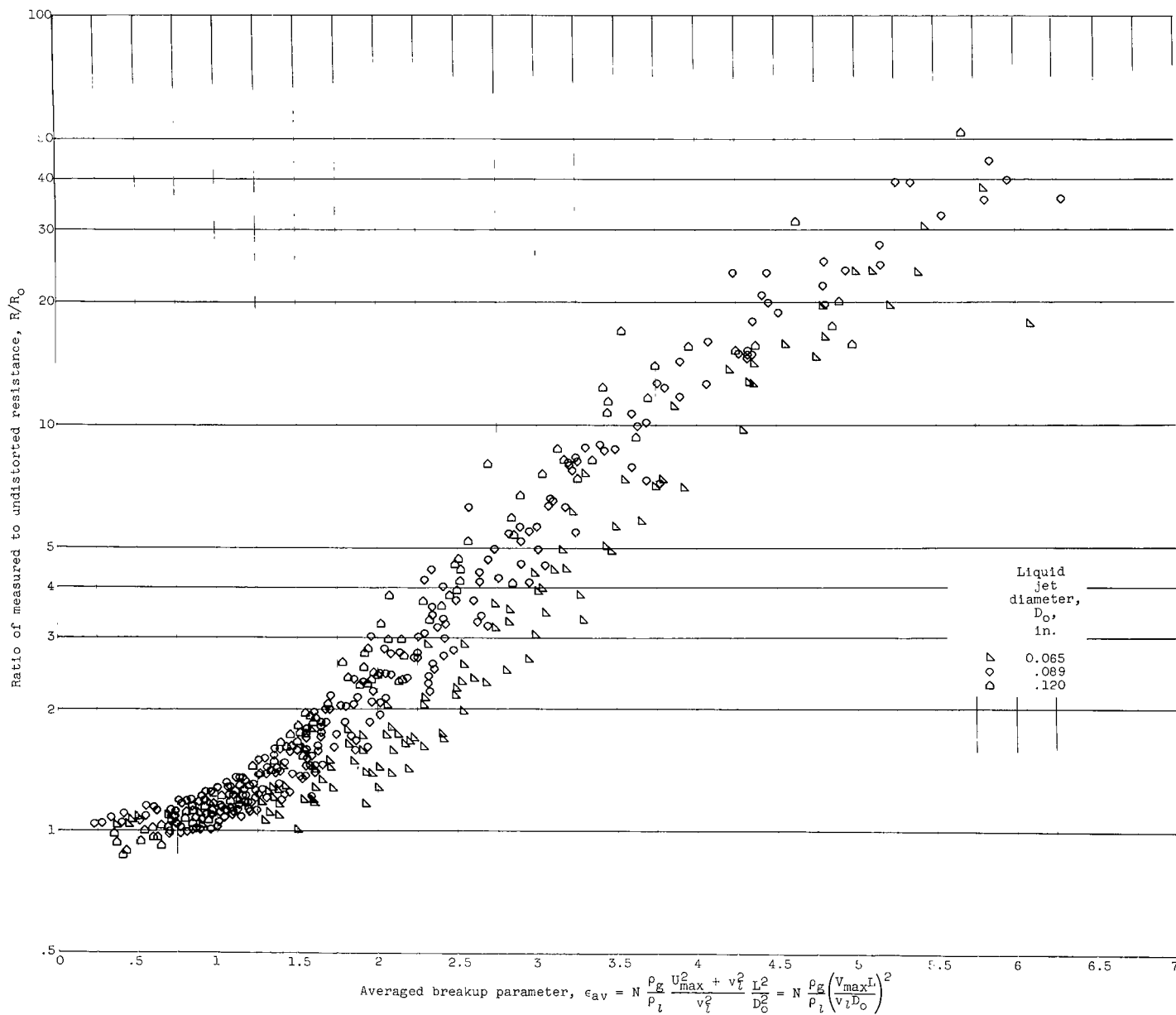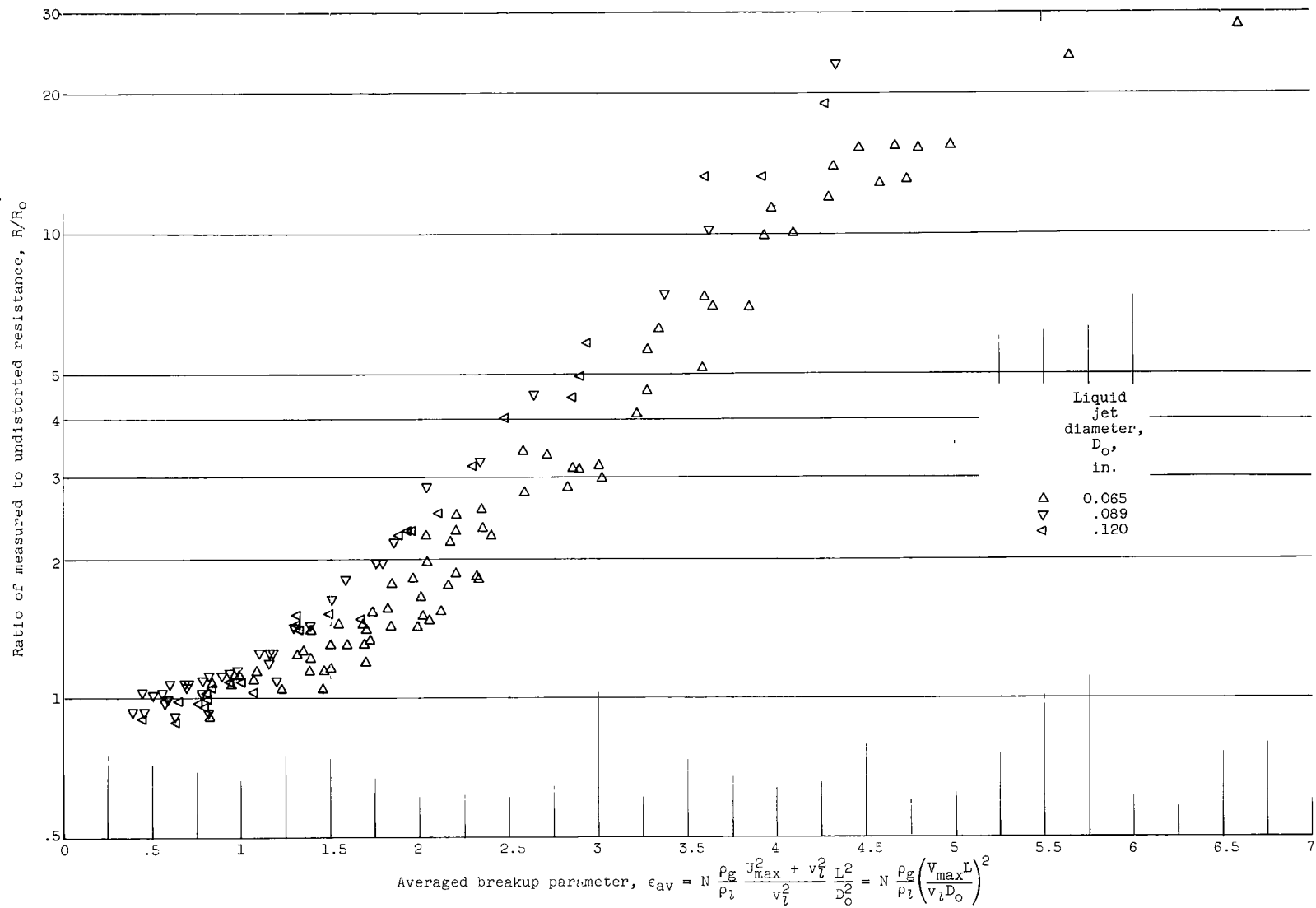Figure 13. - Effect of gas density, gas velocity, liquid velocity, and jet diameter on action time required to give a fixed degree of breakup. Effective action distance, 0.56 inch; ratio of measured to undistorted resistance, 3.

(a) Gas injector, I; approximate effective action distance, 0.35 inch.

Figure 14. - Electrical resistance as function of breakup parameter for various liquid jet diameters.

Ratio of measured to undistorted resistance, R/R_o

30

20

10

5

4

3

2

1

.5

0   .5   1   1.5   2   2.5   3   3.5   4   4.5   5   5.5   6   6.5   7

Liquid
jet
diameter,
D_o,
in.

△	0.065
▽	.089
◁	.120

Averaged breakup parameter, $\epsilon_{av} = N \dfrac{\rho_g}{\rho_l} \dfrac{U_{max}^2 + v_l^2}{v_l^2} \dfrac{L^2}{D_o^2} = N \dfrac{\rho_g}{\rho_l} \left(\dfrac{V_{max} L}{v_l D_o} \right)^2$

(b) Gas injector, II; approximate effective action distance, 0.56 inch.

Figure 14. - Continued. Electrical resistance as function of breakup parameter for various liquid jet diameters.

(c) Gas injector, II'; approximate effective action distance, 0.70 inch.
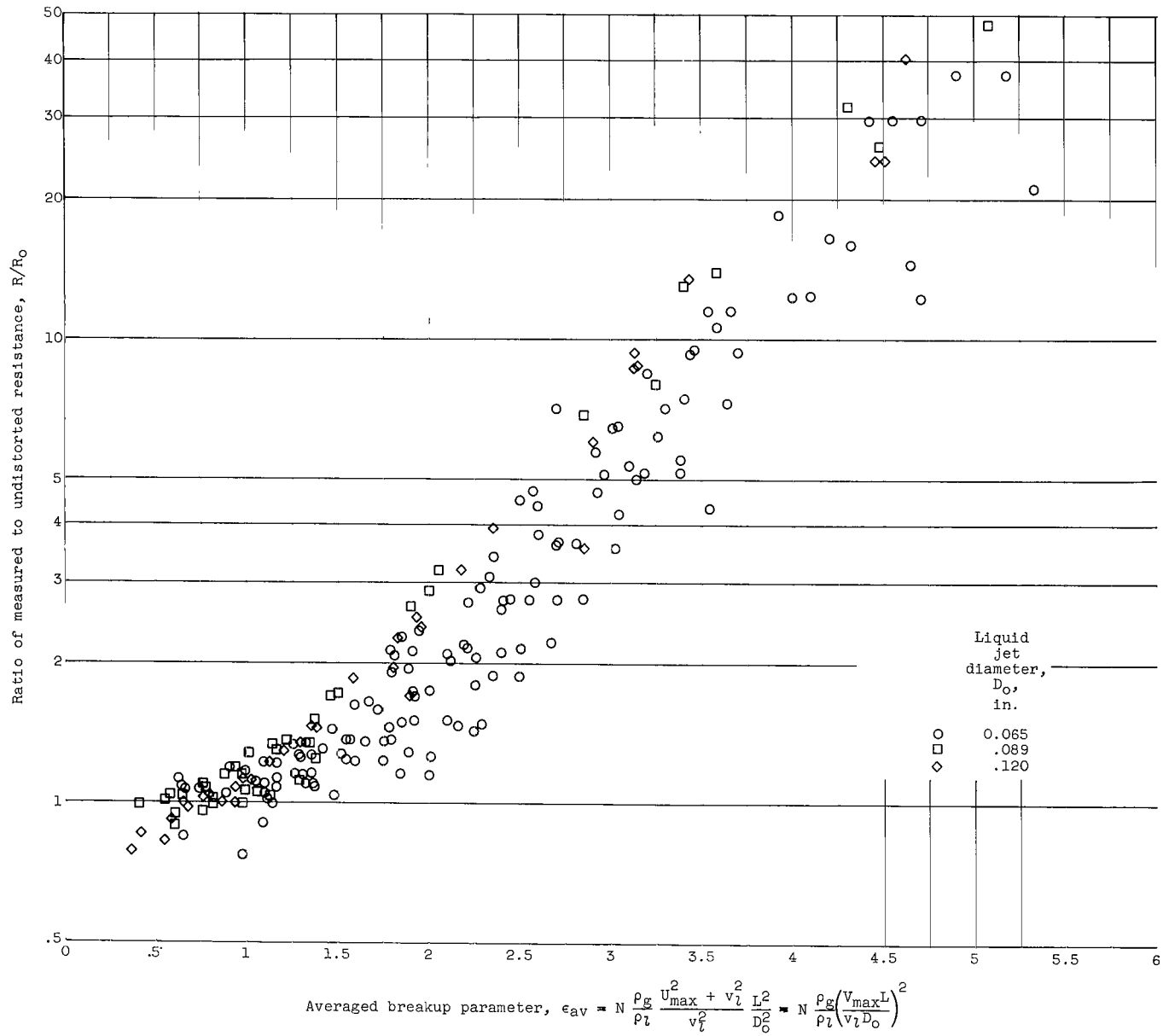
Figure 14. - Concluded. Electrical resistance as function of breakup parameter for various liquid jet diameters.

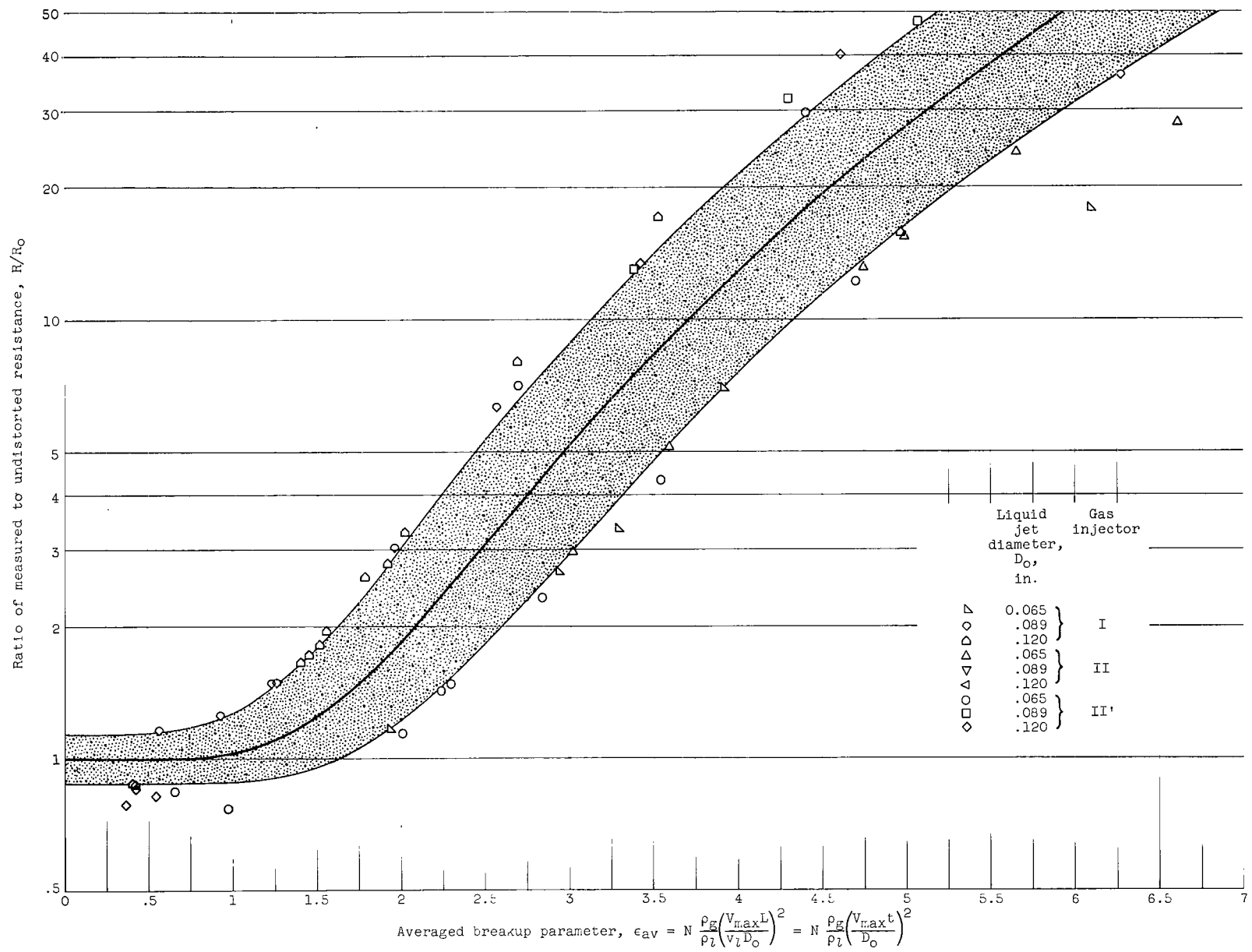Figure 15. - Combined experimental data with assumed average curve. Data falling outside assumed range are plotted individually.
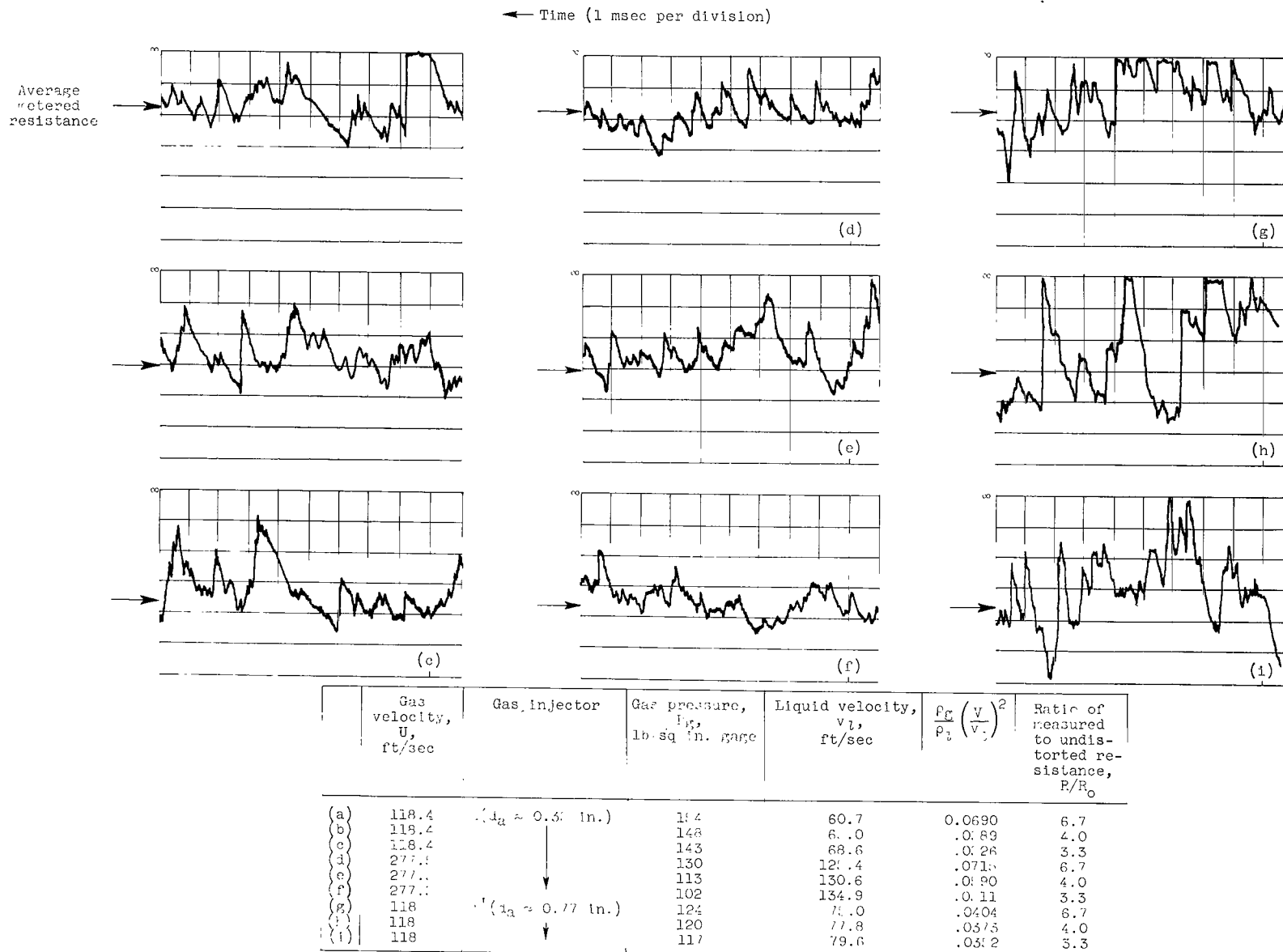
← Time (1 msec per division)

Average
metered
resistance →

(d)

(g)

(e)

(h)

(c)

(f)

(i)

	Gas velocity, U, ft/sec	Gas injector	Gas pressure, P_g, lb·sq in. gage	Liquid velocity, v_l, ft/sec	$\dfrac{\rho_g}{\rho_l}\left(\dfrac{v}{v_l}\right)^2$	Ratio of measured to undistorted resistance, R/R_o
(a)	118.4	$(d_a \approx 0.3\ \text{in.})$	154	60.7	0.0690	6.7
(b)	118.4		148	6..0	.0.89	4.0
(c)	118.4		143	68.6	.0.26	3.3
(d)	277.9		130	12..4	.071.	6.7
(e)	277..		113	130.6	.0.90	4.0
(f)	277..		102	134.9	.0.11	3.3
(g)	118	$(d_a \approx 0.77\ \text{in.})$	124	7..0	.0404	6.7
(h)	118		120	77.8	.0575	4.0
(i)	118		117	79.6	.05.2	3.3

Figure 16. – Oscilloscope records of time-varying resistance of water jets. Orifice diameter, 0.089 inch; orifice length to diameter ratio, 14.
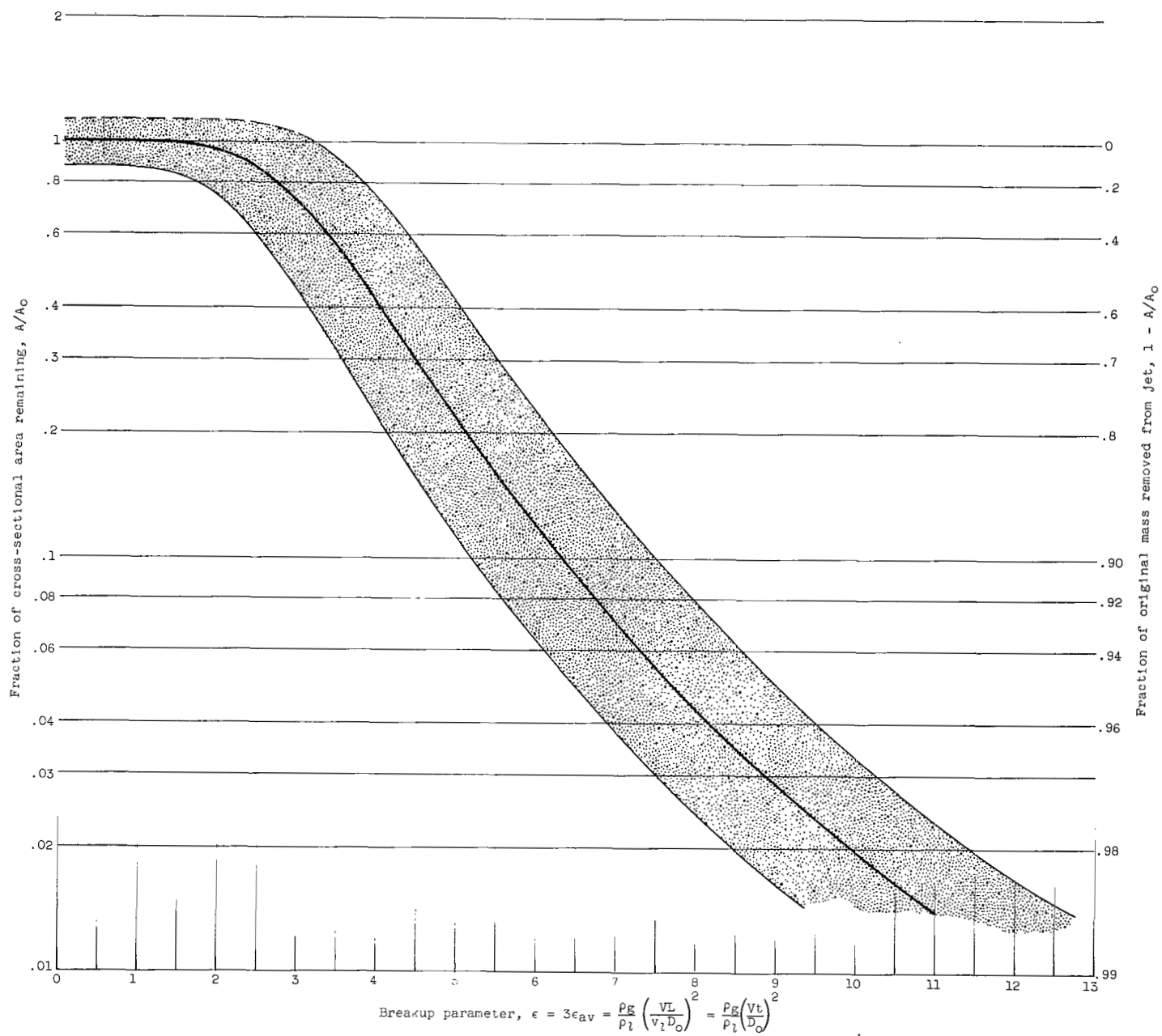
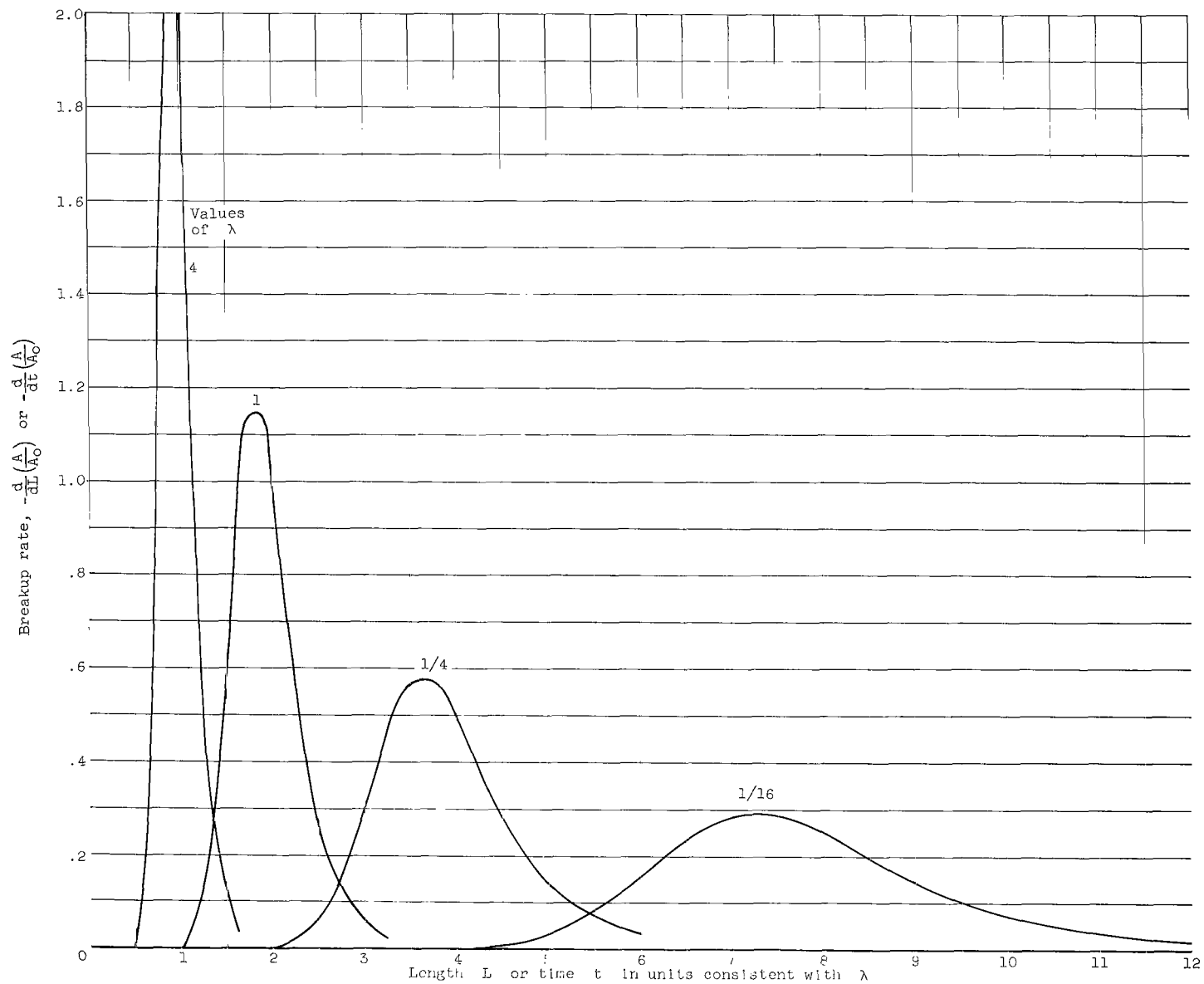Figure 17. - Extent of breakup as function of breakup parameter.

Breakup parameter, $\epsilon = 3\epsilon_{av} = \dfrac{\rho_g}{\rho_l}\left(\dfrac{VL}{v_l D_o}\right)^2 = \dfrac{\rho_g}{\rho_l}\left(\dfrac{Vt}{D_o}\right)^2$

Fraction of cross-sectional area remaining, A/A_o

Fraction of original mass removed from jet, $1 - A/A_o$

Figure 18. - Variation of breakup rate with length or time at various values of λ where $\lambda_L = \dfrac{\epsilon}{L^2} = \dfrac{\rho_g}{\rho_l}\left(\dfrac{V}{v_l D_o}\right)^2$ and $\lambda_t = \dfrac{\epsilon}{t^2} = \dfrac{\rho_g}{\rho_l}\left(\dfrac{V}{D_o}\right)^2$.

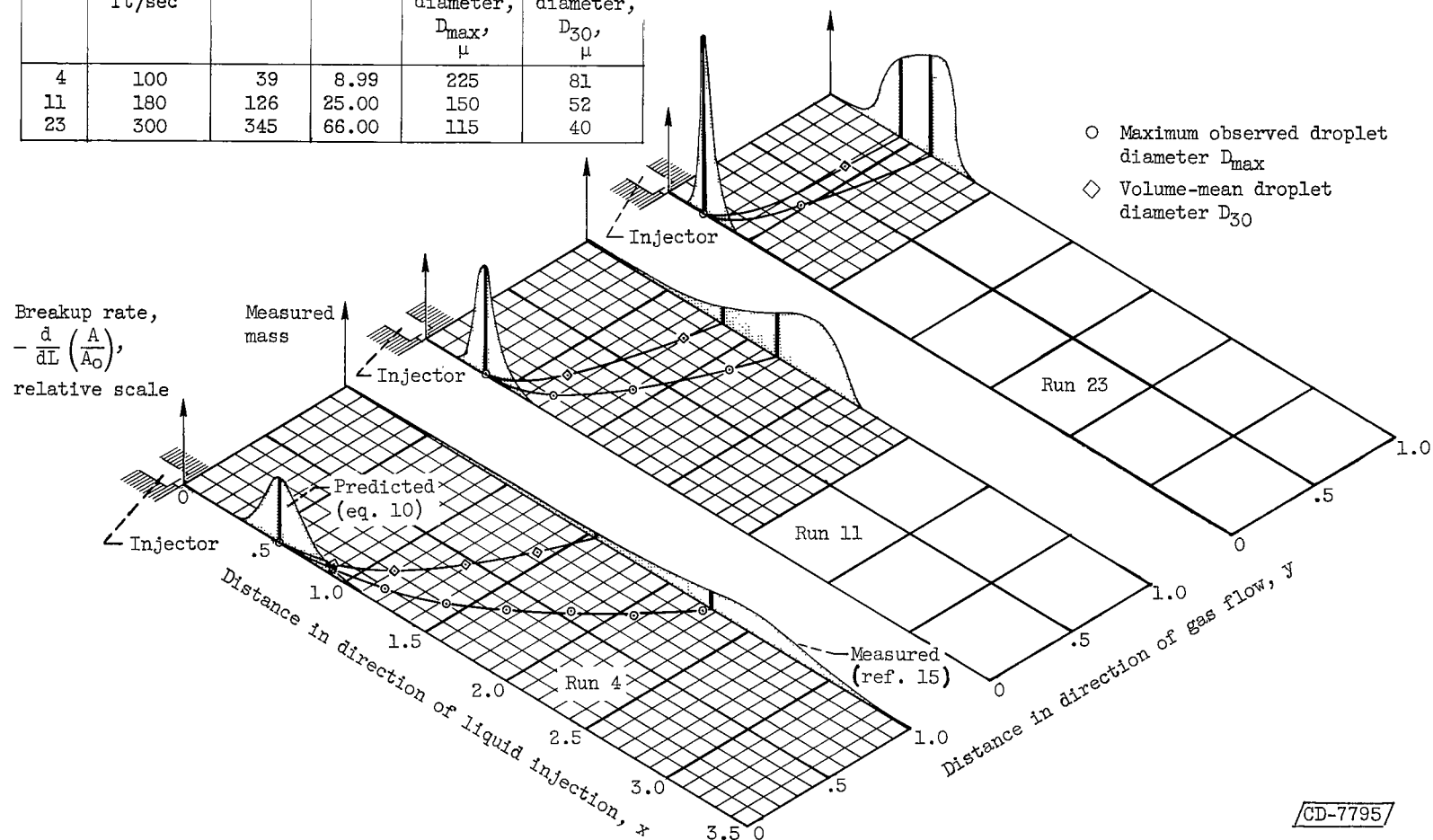| Run	Gas velocity, U, ft/sec	Weber number, We	λ_L per sq in.	Maximum observed droplet diameter, D_{max}, μ	Volume-mean droplet diameter, D_{30}, μ
4	100	39	8.99	225	81
11	180	126	25.00	150	52
23	300	345	66.00	115	40

Figure 19. - Comparison of predicted rate of mass release by breakup of 0.030-inch iso-octane jet at 51-foot-per-second velocity, with mass distributions measured downstream (y = 1.0) in reference 15. Calculated trajectories of maximum and average observed drop sizes and drop positions are shown. Drop positions are shown at 1/2-millisecond intervals.
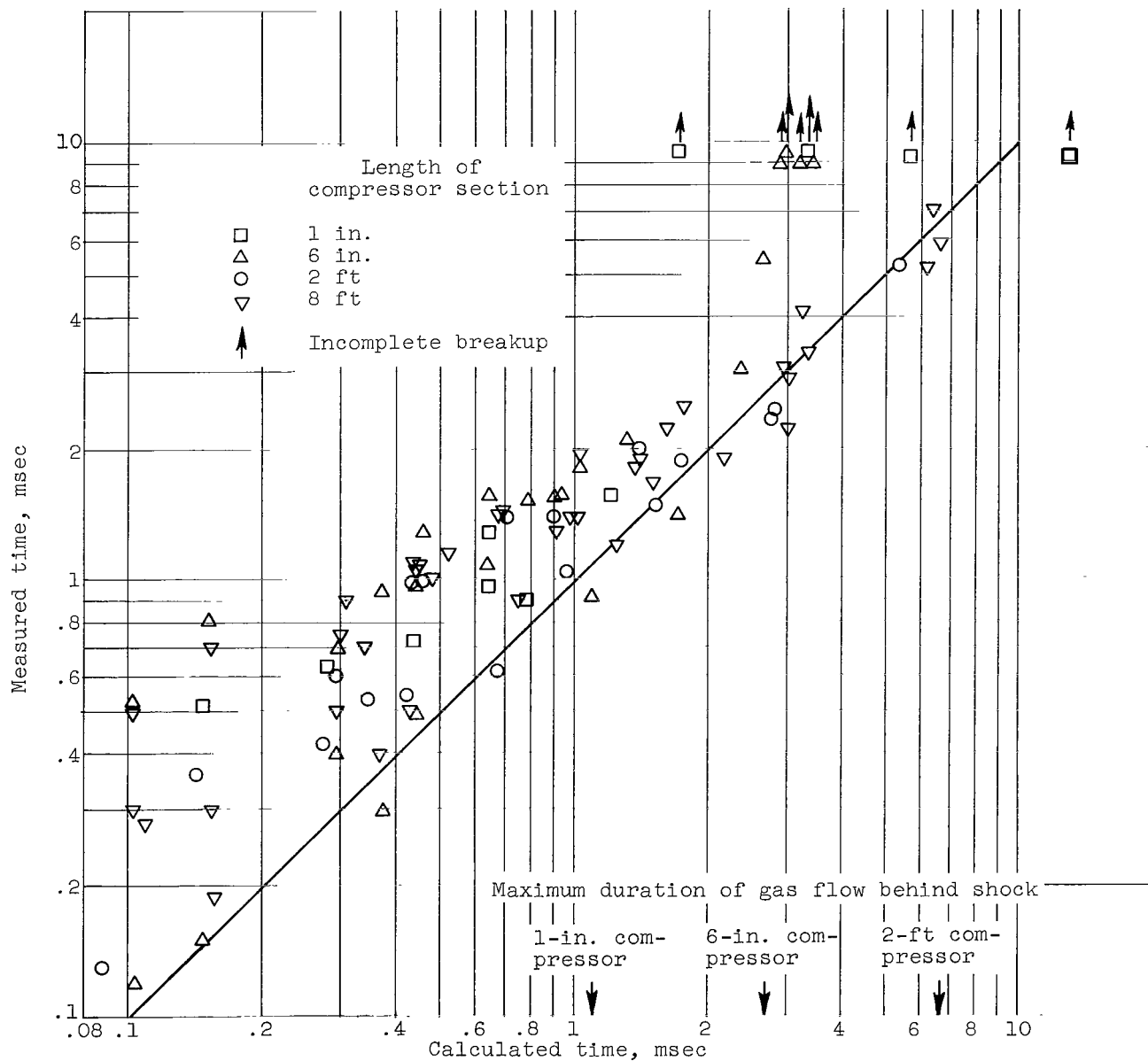
Figure 20. - Comparison of calculated times necessary for 99 percent reduction in area with measured jet breakup times from reference 17.

"The aeronautical and space activities of the United States shall be conducted so as to contribute . . . to the expansion of human knowledge of phenomena in the atmosphere and space. The Administration shall provide for the widest practicable and appropriate dissemination of information concerning its activities and the results thereof."

—NATIONAL AERONAUTICS AND SPACE ACT OF 1958

NASA SCIENTIFIC AND TECHNICAL PUBLICATIONS

TECHNICAL REPORTS: Scientific and technical information considered important, complete, and a lasting contribution to existing knowledge.

TECHNICAL NOTES: Information less broad in scope but nevertheless of importance as a contribution to existing knowledge.

TECHNICAL MEMORANDUMS: Information receiving limited distribution because of preliminary data, security classification, or other reasons.

CONTRACTOR REPORTS: Technical information generated in connection with a NASA contract or grant and released under NASA auspices.

TECHNICAL TRANSLATIONS: Information published in a foreign language considered to merit NASA distribution in English.

TECHNICAL REPRINTS: Information derived from NASA activities and initially published in the form of journal articles.

SPECIAL PUBLICATIONS: Information derived from or of value to NASA activities but not necessarily reporting the results of individual NASA-programmed scientific efforts. Publications include conference proceedings, monographs, data compilations, handbooks, sourcebooks, and special bibliographies.

Details on the availability of these publications may be obtained from:

SCIENTIFIC AND TECHNICAL INFORMATION DIVISION

NATIONAL AERONAUTICS AND SPACE ADMINISTRATION

Washington, D.C. 20546